
Lunds tekniska högskola
Department of Physics

Ultrafast Transient coherent Raman Microscopy (TRaM)

Eric Nilsson

Supervisor: Jörgen Larsson
Assistant supervisor: Carl Ekström
Examinor: Cord Arnold

Degree project report

Abstract

The aim of this project was to construct a measurement setup to be able to measure the decoherence time of optical phonons. Optical phonons lose coherence by decaying to intermediate phonons and eventually to acoustic phonons which can carry heat, which is why measuring the coherence time of optical phonons is important to characterizing heat flow on short time scales.

Ultrashort laser pulses were produced with a Ti:Sapphire laser oscillator and a Michelson interferometer was constructed to split the pulses into pairs and introduce a time delay between the two pulses. To measure the decoherence time the first pulse excites optical phonons in the material and the second pulse probes how much coherence is left in the system by measuring the visibility of the spectral interference fringes on the Raman peak. By varying the delay on the interferometer, the coherence for different pulse delays can be measured and thereby also the amount of coherence left after this time. The measurements were done using a Raman microscope which focused the beam into a $10\ \mu\text{m}$ small spot size on a diamond sample.

The motivation for constructing this particular measurement setup is that a Ti:Sapphire laser oscillator with a sufficiently short pulse duration was already constructed close to a Raman microscope.

Acknowledgements

I would like to thank my supervisor prof. Jörgen Larsson for all the insights I have received and all the hours spent tinkering in the lab. I would also like to thank my assistant supervisor Carl Ekström for always being available and helpful when I needed it. And I also express my deepest gratitude to Åsa Bengtsson for all the help in the lab and Xiaocui Wang for providing me with useful knowledge and relevant literature for this thesis.

Finally I would like to thank my family and my partner and biggest supporter Linnea Lindh.

Popular scientific summary

When measuring temperatures in every day life we use thermometers. For large objects a standard thermometer is sufficient to get an idea of how the temperature is distributed. If the temperature is not constant, but there exist a slow heat flow, the thermometer may also determine which direction the heat flows by measuring the temperature drop in one area and rise in an adjacent area. Temperature and heat flow measurements are important for many practical applications. For example when turning on the oven you don't want your nearby cabinets to be as hot as the inside of the oven, and when driving the car you don't want the seating area to be the same temperature as the engine.

When the objects of interest get smaller, the thermometer has to get smaller as well to be able to resolve the details of the temperature distribution. And when the heat flow fluctuates very fast, the standard thermometer doesn't have time to cool down to make measurements fast enough. For these situation more sophisticated measuring instruments have been constructed. One example of these is the thermocouple where a thin string measures the temperature. This has the advantage of being smaller and thus both being able to resolve finer detail, and also cooling faster to be able to characterize faster fluctuations.

When the objects of interest reach the atomic scale, all of these methods fall short. One such object is the transistor in a modern CPU. One such CPU may contain billions of transistors, and the surface of the whole CPU can be on the order of 100 mm^2 . This means that modern transistors may be as small as hundreds of nanometers! Not only that, but the CPU might perform billions of actions which produce heat every second.

To be able to characterize how heat is generated and how it flows in these systems, even more sophisticated methods have to be constructed. In this project a measurement technique is constructed which uses ultrashort laser pulses with 70 fs ($0.00000000000007 \text{ s}$) duration. These pulses are shot at the material in pairs, where the first pulse makes the material vibrate, and the second pulse sees how the material vibrates at a short time later.

In this manner phenomena on the order of ps (00000000000.1 s) can be measured, which can give us insight into the behaviour of the generation of heat and of heat flow on very small scales.

Contents

1	Introduction	1
2	Theory	2
3	Method	8
4	Results	16
5	Discussions	28
6	Conclusions	30
7	Outlook	31
8	Appendix	34

1 Introduction

When constructing small electrical components, such as transistors in a processor, the properties of heat flow is of great importance. Heat can be transported through crystalline materials through vibrations in the crystal lattice. These high frequency lattice vibrations can be thought of as quasi-particles called heat-carrying phonons.[1]

When illuminating a material with short pulsed lasers on the order of tens of femtoseconds, other types of lattice vibrations called coherent optical phonons can be excited. These optical phonons are vibrations inside the unit cell of the crystal material,[2] as opposed to acoustic phonons where the whole unit cell is translated. These optical phonons decay to phonons with lower frequency called intermediate phonons which in turn keep decaying, and eventually decay to acoustic phonons which can transport heat in the material.[17] Understanding the decoherence time of optical phonons is thus crucial to the understanding of heat flow in materials, as well as electric and acoustic properties.[3]

The goal of this project was to construct a setup to measure the decoherence time of coherent optical phonons. To do this a Ti:Sapphire oscillator with 70 fs pulses was used. The laser beam was sent into a Michelson interferometer[4] where one of the arms was movable using a stepper motor. The Michelson interferometer includes a beamsplitter which splits each pulse into two and sends them in different paths. When both arms of the interferometer have the same length, the two split pulses coincide in time. If the movable arm is shifted the two pulses will have a different path length, and since each pulse will traverse its respective arm length twice, the difference in path length between the pulses will be twice the difference in arm length. Since the pulses travel at the speed of light, this path length corresponds to a time difference of

$$\Delta t = \frac{2\Delta L}{c} \tag{1}$$

where ΔL is the difference in arm length and c is the speed of light.

These pulses were then sent in to a Raman microscope.[5] This microscope focused the beams to 10 μm spots, which allowed for much smaller samples to be measured than had previously been done.

The first pulse, called the pump, induced coherent optical phonons in the material. These phonons then decayed until the second pulse, called the probe, probed the coherence left in the system.

The material of interest in this project was diamond. The reason for choosing diamond is that the band gap of diamond is far from the energy of the 785 nm laser pulses which were used. This is important to not excite any carriers across the band gap of the material, since this takes the force exerted on the material from an impulsive force to a displacive force.[6]

1.1 Young's double slit experiment and spectral interference

When a coherent beam of light is sent onto two thin slits with a separation d , the two slits will act as point light sources sending out spherical wave fronts.[7] When detecting the light on a screen behind the two slits an interference pattern will be visible. This pattern is a periodic pattern in space where the maxima will be separated by

$$x = \frac{z \cdot \lambda}{d} \tag{2}$$

where z is the distance from the slits to the screen and $z \gg d$.

If instead of the two light sources being separated in space, two coherent pulses are separated in time, a similar pattern will emerge in the frequency domain instead of in space, and it is then

called spectral interference.[8] This pattern can be used to determine the coherence in the system after this time.

2 Theory

2.1 Light matter interaction

When light is absorbed by a material, the photon energy is converted to internal energy in the material. If the energy of the photon matches the energy gap between two energy levels of the material, the material can be excited by the photon to the higher of these energy levels. By a process called spontaneous emission the material can then return to its ground state, and at the same time emit a photon, with the same energy as the absorbed photon.

A seemingly similar process is the Rayleigh scattering[9] of a photon. This process also sends out a photon with the same energy as the incoming photon.

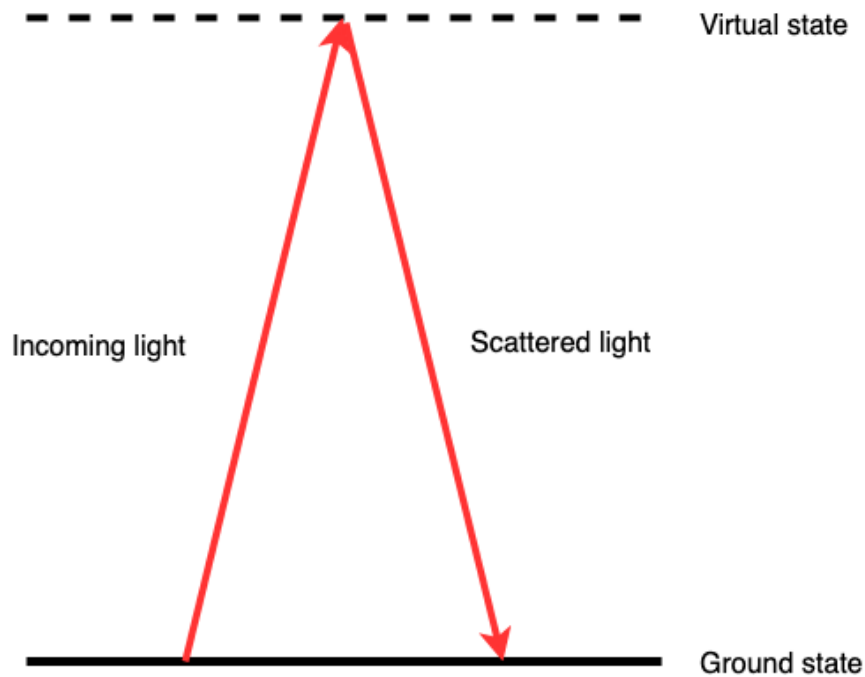


Figure 1: Rayleigh scattering of a photon. The incoming photon is absorbed by a virtual energy level in the material and a photon is then re-emitted with the same energy as the incoming photon when the material relaxes to its ground state.

The most important difference between spontaneous emission and Rayleigh scattering for this report is that the photon does not need to match any energy gap in the material it interacts with. The material is instead excited to a so called virtual energy level as shown in Figure 1. Thus photons of any energy can be Rayleigh scattered, though the probability for scattering might be very low.

The scattering used in the following setup is Raman scattering.[10] As for Rayleigh scattering the material is excited to a virtual energy level, but instead of being relaxed to the ground state

when re-emitting the photon, the Raman process relaxes the material to the first vibrational state. This vibrational energy can be viewed as a quasiparticle called a phonon.[11]

Since the energy of the material is not the same before and after the interaction with the photon, the photon energy must change. If the energy of the emitted photon is lower than that of the incident photon, the scattering is called Stokes scattering, and if the energy of the emitted photon is higher than that of the incident photon, the scattering is called anti-Stokes scattering.

The energy gap between the ground state of the material and the first vibrational state is specific for the material, this means that the energy shift of the photon is also specific for the material.[12]

2.2 Interferometry

For simplicity, we consider the interference of plane waves. The complex amplitude U of a plane wave can be written as $U = \sqrt{I_0}e^{-ikz}$ where I_0 is the intensity of the wave, k is the wave number and z is the direction of propagation.[7] If two electromagnetic waves overlap, they will interfere. We consider two co-propagating plane waves where one of the waves is delayed a distance d . the total complex amplitude of the two waves will be

$$U_{tot} = U_1 + U_2 = \sqrt{I_1}e^{-ik_1z} + \sqrt{I_2}e^{-ik_2(z-d)}.$$

If the waves are identical, except for a phase difference, we can set $I_1 = I_2 = I_0$ and $k_1 = k_2 = k$ and Equation 2.2 then becomes

$$U_{tot} = \sqrt{I_0}e^{-ikz} (1 + e^{ikd}) \quad (3)$$

The intensity of this composite wave is then

$$I_{tot} = |U_{tot}|^2 = 2I_0(1 + \cos(kd)). \quad (4)$$

If the two plane waves are not perfectly aligned, so that one of the waves travel with an angle θ to the other wave, a fringe pattern will emerge due to the interference between the two waves. Let the θ be in the x-z plane, and consider a plane perpendicular to the propagation direction of the waves with $z = 0$. The two waves U_1 and U_2 will then be described as

$$U_1 = \sqrt{I_0} \quad (5)$$

$$U_2 = \sqrt{I_0}e^{-iks\sin(\theta)x}. \quad (6)$$

The resulting intensity is[7]

$$I = |U_1 + U_2|^2 = \left| \sqrt{I_0} (1 + e^{-iks\sin(\theta)x}) \right|^2 = 2I_0 \cos(ks\sin(\theta)x). \quad (7)$$

For small angles θ the intensity can be approximated as

$$I \approx 2I_0 \cos(k\theta x). \quad (8)$$

The contrast of these fringes, called the visibility, is defined as

$$V = \frac{I_{max} - I_{min}}{I_{max} + I_{min}} \quad (9)$$

where I_{max} and I_{min} is the maximum and minimum intensity in the pattern respectively. In a multimode laser, the different modes, or laser frequencies are separated by a frequency $\nu_F = \frac{c}{2L}$ where c is the speed of light and L is the length of the laser cavity[13]. When two waves consisting of multiple frequencies with a separation of ν_F interfere in this manner, the visibility of the fringe pattern is maximized when the path difference of the two waves is zero.

The interferometer used in this project is the *Michelson interferometer*. [4] This interferometer consists of two arms. The mirror on one of the arms can be adjusted as seen in Figure 2. A laser beam enters the interferometer from the left in the picture. The beam then hits a beam splitter, which splits half of the intensity to the top mirror, and half the intensity to the mirror to the right. The split beams are then reflected off of the mirrors and recombined in the beam splitter, where half of the intensity travels back to the incoming laser and half is reflected downward in the picture. As seen in the picture, the difference in path length of the two beams is $2d$ where d is the distance the mirror on the right is moved away from the position where the path length is equal.

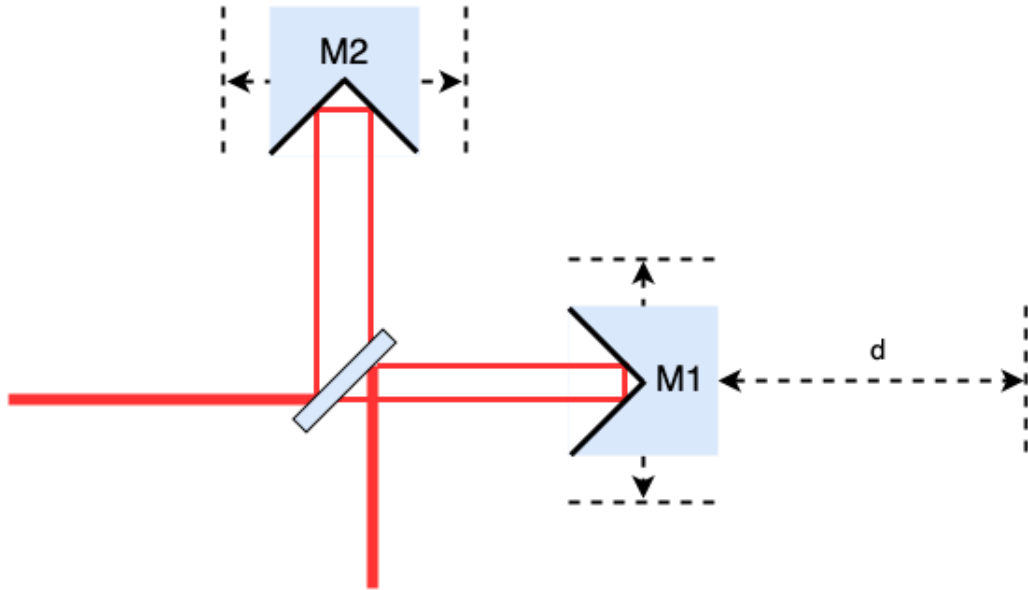


Figure 2: A schematic picture of a Michelson interferometer. The mirror M1 is adjustable. For clarity the back-reflected beams are left out.

There will be a maxima in visibility when the path difference is 0.

For the measurements in this project a pulsed laser was used. In the way described above, the pulses were split and recombined. Since the speed of light is known, the distance between the outgoing pulses can be interpreted as a time delay $\Delta t = 2d/c$ where c is the speed of light. The duration of the pulses is 70 fs. For a pulse pair to interfere they have to overlap spatially which means that for a pulse pair to show an interference pattern the delay between the two pulses must be less than the pulse duration.

2.3 Raman spectroscopy

Raman spectroscopy[15] is a very common technique that is used to characterize materials. A sample is exposed to laser light with a narrow bandwidth and the scattered light is analyzed

with a spectrometer. The spectrometer in the Raman microscope used in this project uses reflective gratings and two curved mirrors. This setup is shown in Figure 3. The light is slightly divergent when it passes through the entrance slit. The first curved mirror collimates the light and the light then hits the diffraction grating, covering a large surface area due to being allowed to diverge before the first curved mirror. There are three gratings included with 150 grooves per mm, 1200 grooves per mm and 2400 grooves per mm, which will be referred to as 150g, 1200g and 2400g respectively. The reflected light follows the grating equation

$$\sin\theta_q = -\sin\theta_i + \frac{q\lambda}{\Lambda} \quad (10)$$

where Λ is the distance between adjacent grooves, q is the order of the reflected or transmitted light and θ_i is the angle of the incoming light.

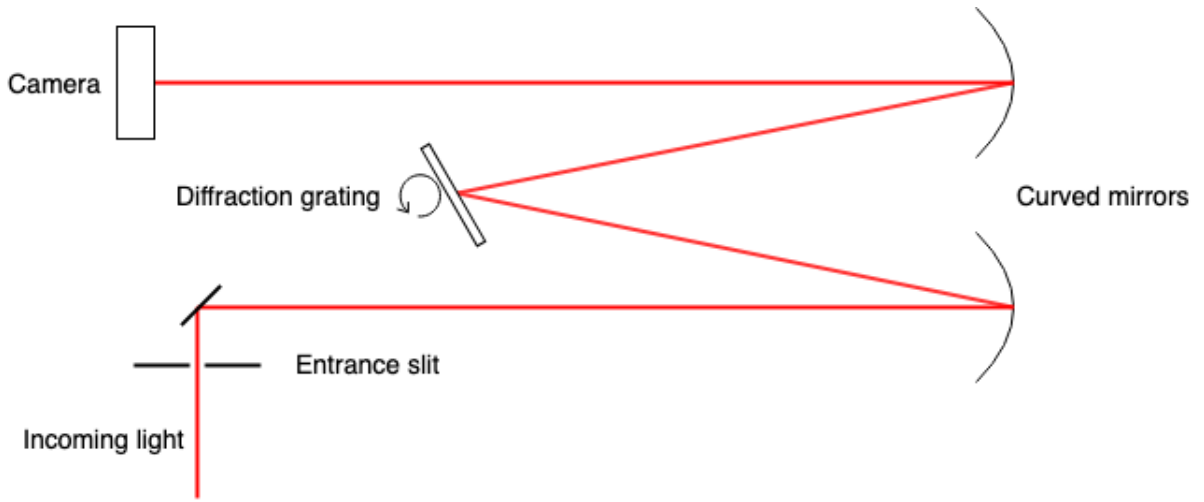


Figure 3: A schematic picture of a spectrometer with incoming white light being separated into its spectral components.

When the light scattered from the sample hits the diffraction grating, it follows from Equation (10) that light with longer wavelengths is deflected more. Since the light of different wavelengths are leaving the grating at different angles, a distance away from the diffraction grating the different wavelengths are separated in space. The light then hits the second curved mirror and is refocused. The light is then captured by an Andor Zyla sCMOS camera and the spectrum of the scattered light can be analyzed.

The change in energy of the outgoing photons compared to the incoming photons for Raman scattering is specific to the material which scatters the light.[14] This means that the energy off-set of the scattered light characterizes the sample. This is shown as the energy difference between the ground state and the first vibrational state in Figure 4. For Raman spectroscopy the spectrum is measured in wavenumbers, k , in the unit relative cm^{-1} where $1 \text{ eV} = 8065.5 \text{ cm}^{-1}$ for photons. By rotating the grating the angle θ_i in Equation (10) is changed, which in turn changes the outgoing angle θ_q . The location where a certain wavelength hits the camera is then shifted. The grating is rotated so that the incoming light corresponds to 0 relative cm^{-1} . The Raman peaks specific for the sample material can then be directly read out as relative cm^{-1} where relative means relative to the incoming light. For this report the studied material is diamond, which has a Raman peak at 1332 cm^{-1} . [15]

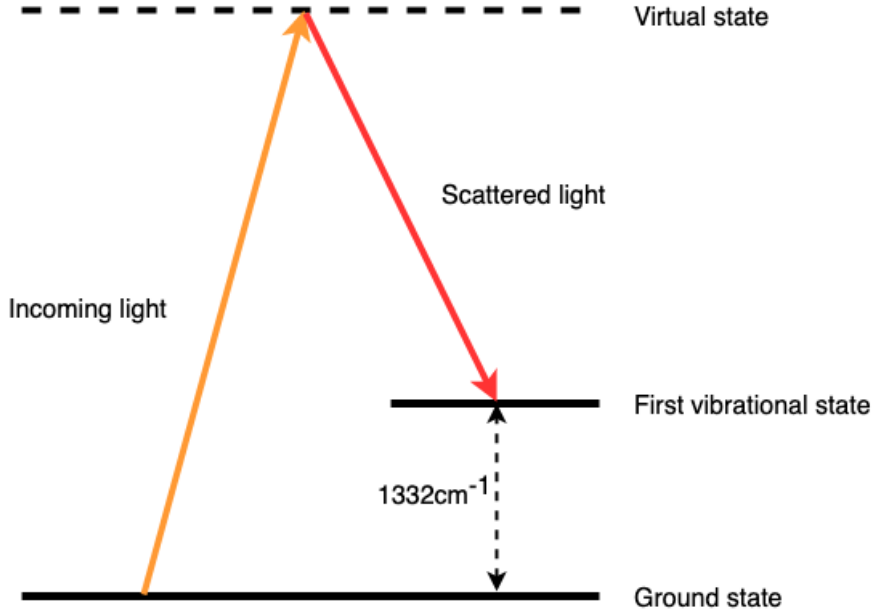


Figure 4: Raman scattering process for diamond.

The wavenumber $\tilde{\nu} = \frac{1}{\lambda}$ where the unit for $\tilde{\nu}$ is cm^{-1} and for λ is m. Taking the derivative of $\tilde{\nu}$ with respect to λ yields

$$\frac{d\tilde{\nu}}{d\lambda} = -\frac{1}{\lambda^2} \implies d\tilde{\nu} = -\frac{1}{\lambda^2} d\lambda$$

inserting $d\lambda = 1 \text{ nm}$ and $\lambda = 785 \text{ nm}$ then gives that a change of 1 nm at 785 nm corresponds to 16.22 cm^{-1} . In the rest of the report it is assumed that this is true in the whole spectral region of the measurements.

2.4 Spectral interference

For measuring the coherence time of the coherent phonons induced by the Raman scattering process a pump-probe technique is used. As described in the previous section a pair of light pulses is generated and the time delay between the pulses is controllable. If a photon in the first pulse in a pulse pair, called the pump, is Raman scattered, coherent optical phonons are excited in the sample.[16] These optical phonons then may split into two acoustic phonons and lose coherence[17] before the second pulse, called the probe, reaches the sample. If a photon in the second pulse also interacts with the sample via Raman scattering, the coherence of the phonons is probed.

The combined Stokes field of the two scattered fields can be written as

$$E_{\text{stokes}} = E_1 + E_2$$

where E_1 is the Stokes pulse from the pump pulse and E_2 the Stokes pulse from the probe.[18] The second Stokes pulse is dependent on the first pulse and the maintained coherence of the phonons, and can therefore be expressed as $E_2(t) = e^{i\theta} E_1(t - \tau)$ where τ is the delay between pulses and θ is the spontaneous fluctuating phase difference between the pulses[18] so the total Stokes field can be written as

$$E_{stokes}(t) = E_1(t) + e^{i\theta} E_1(t - \tau).$$

Fourier transforming this expression gives

$$|E_{stokes}(\omega)|^2 = 2|E_1(\omega)|^2(1 + \cos(\omega\tau + \theta))$$

which is the same interference pattern as in Equation 8 except for a phase θ , but spectrally instead of spatially. The expectation value of this field is

$$\langle |E_{stokes}|^2 \rangle_{shots} = 2|E_1(\omega)|^2(1 + e^{-\Gamma|\tau|} \cos(\omega\tau)) \quad (11)$$

where Γ is the linewidth of θ , assuming a Lorentzian distribution. The difference in angular frequency between two maxima of the interference pattern satisfies $d\omega = 2\pi$. Since $\omega = 2\pi f = 2\pi \frac{c}{\lambda}$, we can differentiate this expression with respect to λ and obtain

$$d\omega = -2\pi \frac{c}{\lambda} d\lambda$$

which gives a period in wavelength of

$$d\lambda = \frac{\lambda^2}{c\tau}. \quad (12)$$

This relationship is shown in Figure 5.

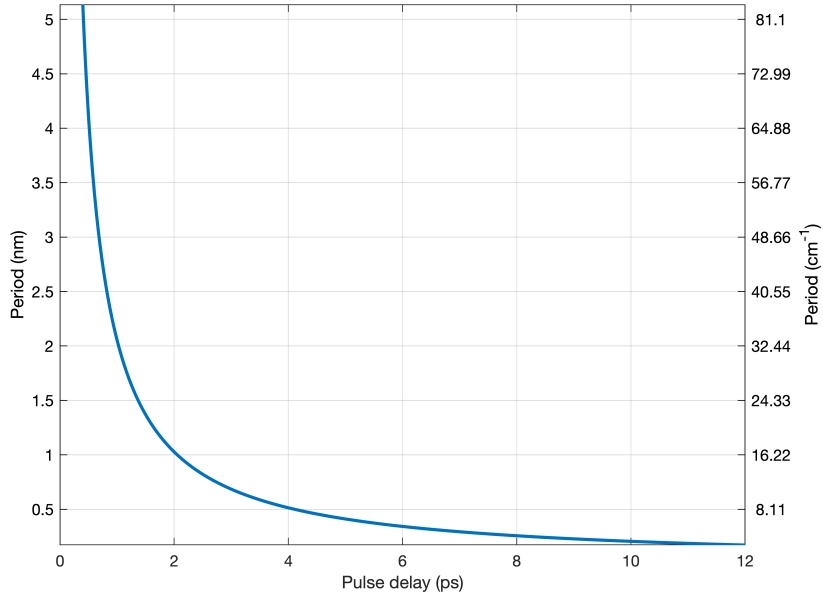


Figure 5: The period of the interference pattern plotted against the delay between the pulses.

The visibility of this pattern is calculated by inserting Equation (11) into Equation (9)

$$V = \frac{(1 + e^{-\Gamma|\tau|}) - (1 - e^{-\Gamma|\tau|})}{(1 + e^{-\Gamma|\tau|}) + (1 - e^{-\Gamma|\tau|})} = e^{-\Gamma|\tau|}. \quad (13)$$

From Equation (13) we see that the visibility of the fringe pattern decreases exponentially with increased pulse delay. The visibility is dependent on the phonon coherence, which means that the decoherence time for the phonons is [19]

$$T = \frac{1}{\Gamma}. \quad (14)$$

3 Method

3.1 Optical setup

3.1.1 Michelson interferometer

The main part of the project was the construction of the Michelson interferometer, which is shown in Figure 7. The essential components of the interferometer were two mirrors and a beamsplitter. The mirrors were two corner gold mirrors, where each mirror was designed so that two quadratic mirrors were connected at a 90 degrees angle. These mirrors were chosen instead of flat mirrors since the 90 degree angles make them insensitive to rotation in the horizontal plane. This is shown in Figure 6 for the same mirror when it is perfectly aligned and when it has been mis-aligned by 10°. As seen, the reflected beam is always anti-parallel to the incoming beam in these mirrors. The reason this was preferred over regular flat mirror, was because both mirror M1 and M2 in Figure 2 were mounted on translation stages which could slightly rotate the mirrors when moving the mirrors. This was especially true for mirror M1 which was moving every time the pulse delay had to be altered. The mirrors had a reported tolerance of 10 arcsec.[20] Assuming the total optical path length between the mirrors and the microscope is 10 m, this corresponds to a shift of 0.5 mm which is well below the diameter of the beam before the microscope. This tolerance was therefore acceptable for this purpose.



Figure 6: A schematic of a non-rotated and rotated corner gold mirror reflecting a laser beam.

The mirrors were held by mounts which allowed for tilting to adjust the outgoing beam's angle in respect to the horizontal plane. Both mirrors were mounted on translation stages which allowed for adjustment in the horizontal plane perpendicular to the incoming beam. This was necessary to make the spacing between the incoming and outgoing beam equal for the two mirrors. Mirror M1 in Figure 2 was also mounted on a motorized translation stage which allowed for horizontal movement up to 50 mm parallel to the incoming beam. This motorized translation stage was necessary to adjust the time delay between the outgoing pulses from the interferometer. This was the mirror connected to the adjustable arm of the interferometer.

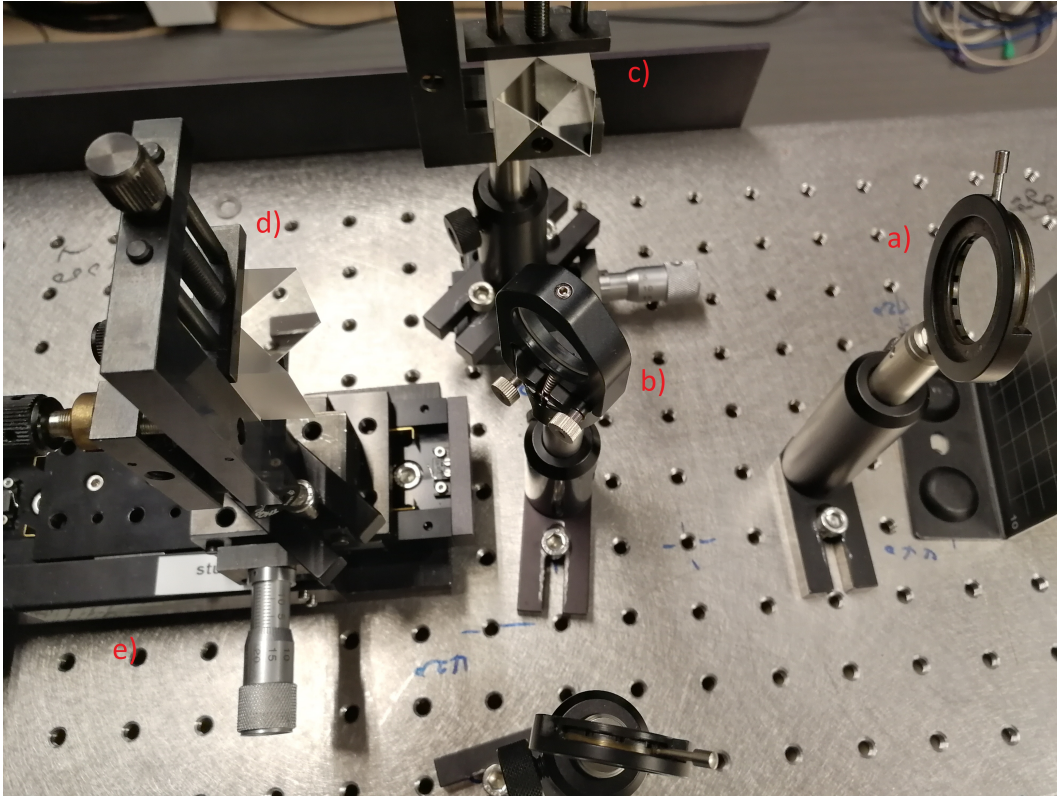


Figure 7: The Michelson interferometer. a) the last aperture for aligning the beam before the Michelson interferometer b) the 50/50 Beam Splitter mounted in an adjustable flip mount c) the stationary mirror mounted on a linear translation stage which can move the mirror laterally d) the movable mirror mounted on both a linear translation stage to move it laterally and on e) a motorized 50 mm translation stage changing the beam path length.

The beamsplitter was mounted with a 45 degree rotation to the incoming beam. This split the incoming beam and half the intensity was directed 90 degrees to the incoming beam where mirror M2 was placed and half the intensity passed right through to the adjustable arm of the interferometer where mirror M1 was placed. The beamsplitter was mounted in an adjustable flip mount. When the mount was flipped the beamsplitter was moved out of the beam so that no light was split to the 90 degrees direction where mirror M2 was.

3.1.2 Introducing oscillator beam into Raman microscope

To introduce the oscillator beam to the setup the alignment laser was removed. The laser that was used for the measurements was a Ti:Sapphire oscillator shown in Figure 8 run in a Kerr-lens mode-locked mode.[21]

The two spherical mirrors in the laser cavity are placed closer together than is optimal for CW operation of the laser which means that the image of the gain medium will be moved further behind the end mirrors. The Ti:Sapphire gain medium exhibits the Kerr effect when exposed to high intensity. Since the intensity profile of the laser beam is gaussian, the gain medium will act as a positive lens for high intensities[22], which moves the image of the amplifier crystal back to the optimal distance from the end mirrors. This makes the laser cavity more stable for

high intensities. When running the laser in CW mode, the laser modes have random phases. By disturbing the lasing, the phases of the laser modes are scrambled, and some modes may happen to be in phase. This creates a pulse train of higher intensity[23] in the laser which will be more stable than the rest of the laser modes. Since this phase now is preferable, more modes will start to oscillate in phase with this pulse train and the laser is mode locked.

When mode locked, the laser beam had a power around 200 mW with 70 fs long pulses and a 100 MHz repetition rate. This gives an average pulse energy of

$$\bar{E}_{pulse} = \frac{200 \text{ mW}}{100 \text{ MHz}} = 2 \text{ nJ}. \quad (15)$$

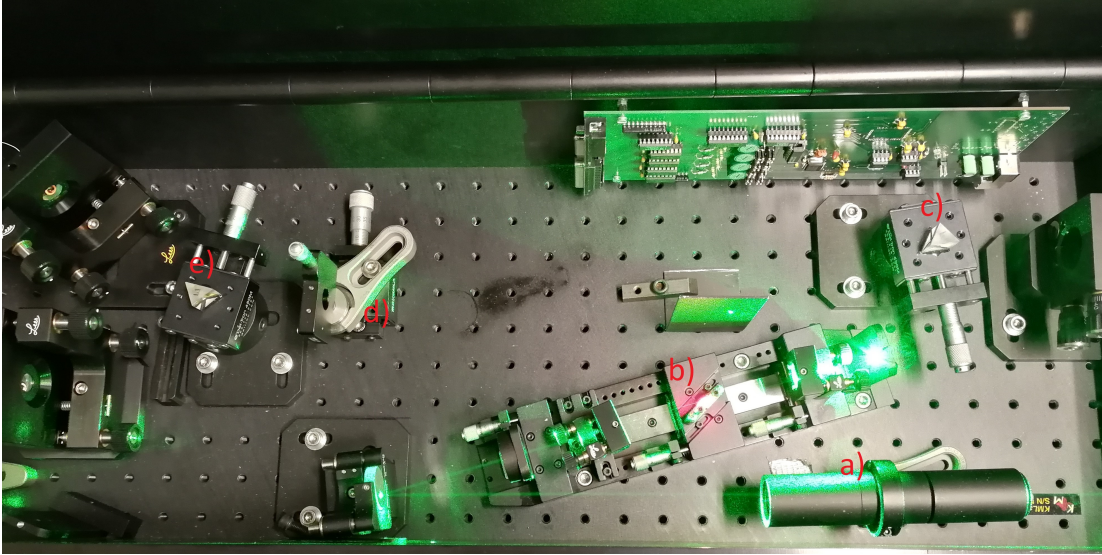


Figure 8: The Ti Saphire oscillator. a) the entrance for the green pump laser b) the Ti Saphire amplifier crystal c) a prism used to shape the beam profile d) a slit e) another prism used to both shape the beam profile and to mode lock the oscillator.

The green pump beam enters the oscillator and is reflected onto the amplifier crystal. This crystal is enclosed in a laser cavity causing lasing when the crystal is pumped. The two prisms shown in the figure were adjusted to get a narrow spectral profile, and the prism e) was pushed down to initialize mode locking. To get the maximum power into the measurement setup, the pulse shape was optimized to the particular bandpass filter that was used. This meant compressing the pulse energy profile in the frequency domain, to concentrate as much output power as possible inside the desired wavelength window. For the 3 nm bandpass filter that was used to get a sharp Raman signal a profile very narrow and sharp in the frequency domain was obtained which served to compress as much power as possible in the 3 nm window around 785 nm. When the power out of the laser was around 200 mW, around 34 mW passed through the 3 nm band pass filter when this profile was achieved. The downside of this profile was that the fringes that modulate the Raman signal are more easily discernable on a wider, flatter Raman signal and this profile had a very sharp peak in the frequency domain.

When using a 10 nm bandpass filter the oscillator was tuned to output a spectral profile that was wider, more flat in the frequency domain. The purpose of this profile was to compress as much energy as possible inside a 10 nm window centered at 780 nm, since all the power outside

this window would be lost, while at the same time get rid of the sharp peak that is present in the profile used for the 3 nm bandpass filter. With the same output power of the laser around 40 mW passed through this bandpass filter.

A Schott RG-715 color filter was inserted in the beam path to filter out the green pump laser light. After the color filter a half-wave plate was inserted to change the polarization of the oscillator beam from horizontally to vertically polarized light to match the lasers inside the Raman microscope.

After the two last apertures after the interferometer a mirror was mounted which directed the beam 90 degrees, which made the beam exit the optical table perpendicular to the edge of the table. An optical rail was mounted to the wall and two mirrors were placed on this rail, the first mirror angled the incoming beam to travel parallel to the wall and the second mirror again angled the beam 90 degrees, this time into a hole that was drilled in the wall to the adjacent room. On the other side of the hole was another optical rail where two mirrors were placed, these mirrors were adjusted to direct the beam down to an optical table where two additional mirrors were placed. These four mirrors are the first mirrors in the laser path in Figure 9. The last two of these mirrors are gold mirrors, and the rest of the mirrors in the entire setup, except for the two gold corner mirrors in the Michelson interferometer, are silver mirrors.

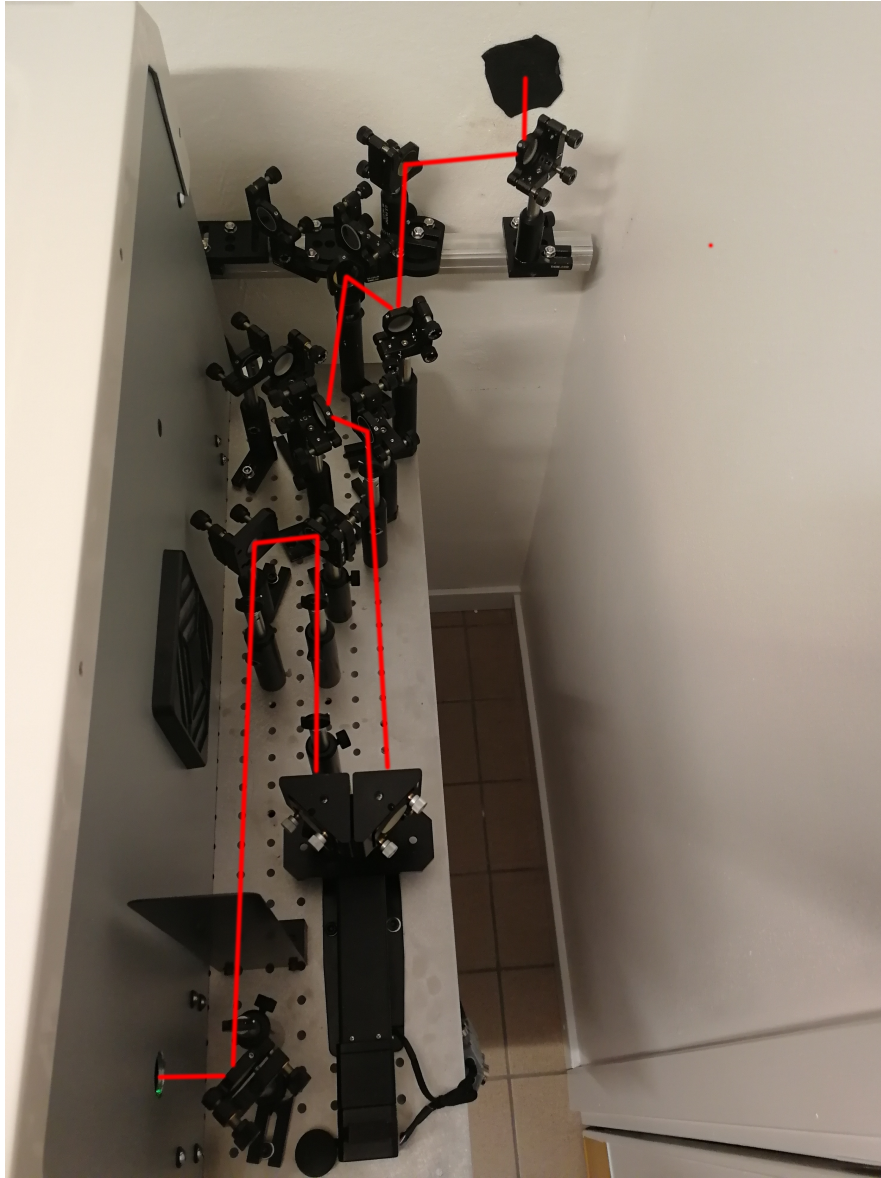


Figure 9: At the top right of the figure is the whole in the wall between the two rooms, in the picture it is covered with black tape. The red line indicates the path of the laser into the Raman microscope.

The last of these two mirrors was mounted on a flip mount and put in the path of an already aligned laser.

The Raman microscope was then turned on and ND filters totaling 8ND was activated. A thin diamond wedge was inserted under the objective lens of the microscope. The focus of the microscope was adjusted until the diamond wedge was in focus with 20x magnification. The ND was then reduced one at a time until the laser spot was visible on the Raman microscope's imaging camera. The Raman microscope camera was then turned off and the beam was directed into a spectrometer. Looking at the Rayleigh peak of the spectra, the two mirrors before the

Raman microscope were adjusted to maximize the incoming intensity.

Due to the beam being divergent and too wide a telescope was constructed in the beam path.

When the beam had passed through all of the optics in the setup, including the initial bandpass filter, the interferometer, the Raman microscope and all the mirrors, just before the sample, the power had reduced to around 9 mW. This reduction in power was mostly due to the interferometer, which by design reduces the power by at least half. The rest of the reduction was probably from the losses when being reflected by the mirrors.

3.1.3 Adjusting the arm length

The purpose of the whole setup was to control the delay between two pulses. To do this effectively one would want to know when the delay between pulses equals 0. Since the delay between the pulses is proportional to the difference in arm length of the interferometer, this corresponds to knowing when the length of the arms are the same.

This was achieved using interferometry. A screen was placed after the interferometer and a negative lens with a short focal length was placed in the beam path before the screen, this enlarged the spot size on the screen. The oscillator was then set to run in CW mode and the motorized translation stage was adjusted until interference fringes were visible. The translation stage was then further adjusted to make the visibility of the fringes as high as possible. When the visibility of the fringes was determined to be maximized, the laser was mode locked. Two 70 fs pulses now had to be overlapped to detect interference fringes which theoretically corresponds to a precision of 21 μm . To do this the translation stage very slowly scanned across a region close to where the maximum of the CW interference fringes was. When interference fringes now were visible the program was paused and the arm length was noted as the end point of an interval where the pulses possibly were overlapped. The translation stage then scanned in the opposite direction and was paused again when fringes were visible. Knowing the two endpoints, the arm length was then manually moved in individual steps in this interval until fringes were visible. The length was further adjusted until the visibility of the fringes were maximized, and the interval of maximum visibility spanned approximately 3 μm .

3.2 Computer code

3.2.1 Matlab

The collected data of the spectral fringes on the Raman peaks was expected to be a series of slightly noisy trigonometric functions.[18] To easily process the data, a Matlab script was written to fit a cosine function to the recorded oscillations. This was done to be able to read out the amplitude and off-set from zero of the oscillations to calculate the visibility. Since the relative phase was unimportant, the script first set the lowest frequency to 0. The data was then fitted to a cosine function using the matlab command `lsqcurvefit` with the amplitude, phase, off-set and period as variables to fit. The guess for the amplitude was done simply by subtracting the minimum value from the maximum value, the guess for the off-set was done equally simply by calculating the mean value of all the points. The guess for the phase was set to 0. The guess for the period was done in two ways. Both ways used the Matlab command `findpeaks` to find the position of the maxima of the function. The first way of calculating the period was done using $\lambda = \frac{\lambda_{max} - \lambda_{min}}{N_{peaks} - 1}$ where max and min refers to the peak with the maximum and minimum wavelength respectively and N_{peaks} is the number of peaks. The second way of calculating the period was done by calculating the period for all peaks and taking the median value as the guess.

To make the lsqcurvefit more robust, the function was first fitted using the first period guess. If the residual of the lsqcurvefit function was too large, the function then tried the second guess and chose the one with the smallest residual.

3.2.2 LabVIEW

A LabVIEW program was designed to automate the data acquisition process. Since the measurements were supposed to be done in succession with a set time delay difference between subsequent acquisitions, and for the same acquisition time for each acquisition, the program allowed the user to set a minimum time delay, a maximum time delay, the acquisition time and the number of acquisitions. The program then moved the delay stage to the distance corresponding to the minimum time delay, then waited for the set acquisition time, before stepping fast to the next time delay and staying there for the same time. This was then repeated until the maximum time delay was reached. Using this method, the acquisition on the Raman microscope could be synchronized with the LabVIEW program, using the same acquisition time on the Raman microscope. Much of the code was repurposed from a template that was included for the translation stage.

3.3 Measurement protocol

The measurements were done by first inserting a sample in the Raman microscope. This is shown as "Sample" in Figure 11. The internal camera was then turned on and the position of the sample was adjusted until the sample was in focus. When the camera was turned on the rod named "Camera arm" in Figure 11 was inserted. This arm had a mirror attached to it which redirected the light from the sample into the camera. The ND filters were then lowered until the beam was visible, and the sample was raised so that the laser spot was as visible as possible. The laser spot on the sample is shown in Figure 10.

The camera was then turned off and the scattered light was instead aimed into the internal spectrometer. The ND filters were removed and the measurements were taken around 1332 cm^{-1} relative to the Rayleigh peak where the Raman peak for diamond was expected to be. Before the acquisition of the data, a background spectrum had to be taken for each new setting.



Figure 10: Picture from the microscope view when the laser spot was as visible as possible on the sample

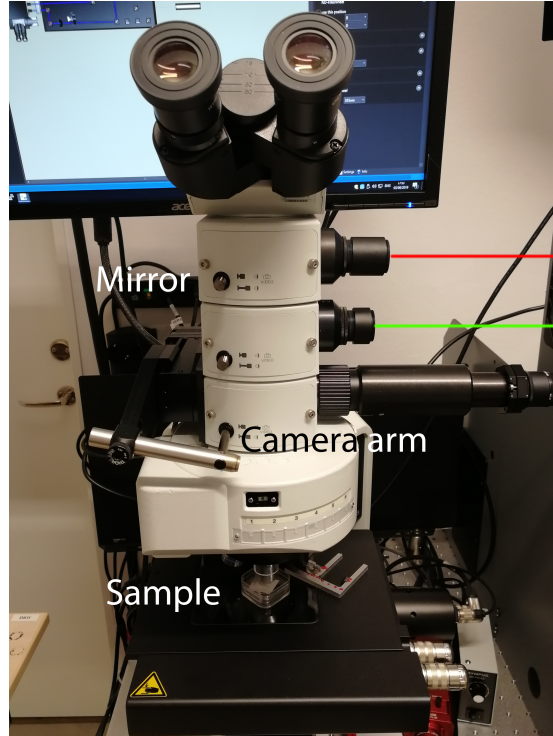


Figure 11: Front view of the microscope. The red line indicates the laser light entering the microscope and the green line indicates the light exiting the microscope.

This was done by pulling out the mirror which is the rod labeled "Mirror" in Figure 11 and then acquiring a background spectrum. This mirror directed the light from the sample into the exit hole which is indicated by a green line. To acquire a spectrum the mirror was inserted again.

4 Results

4.1 Michelson interferometer

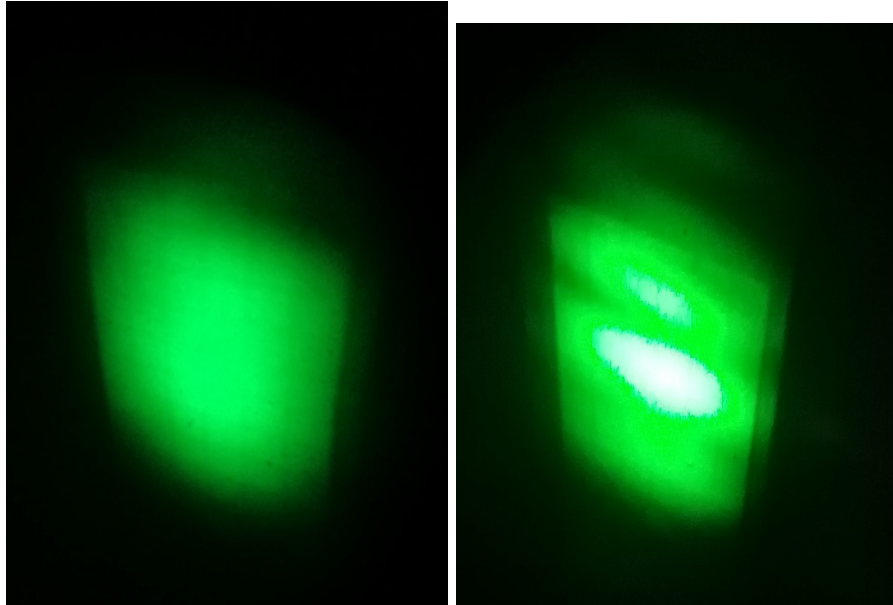
When spatial overlap of the two beams exiting the interferometer was achieved, the interferometer had to be calibrated so that the exact time delay between pulses could be set. In Figure 12 the signal exiting the interferometer is shown after being magnified by a highly concave lens. The following images of the signal are taken of a screen put in the beam path. The images are taken through a IR-viewer which displays the captured light in green.

In Figure 12a there are no visible interference patterns. When moving the translating mirror, weak interference patterns emerged as seen in Figure 12b. This indicated that the path length difference was decreasing.

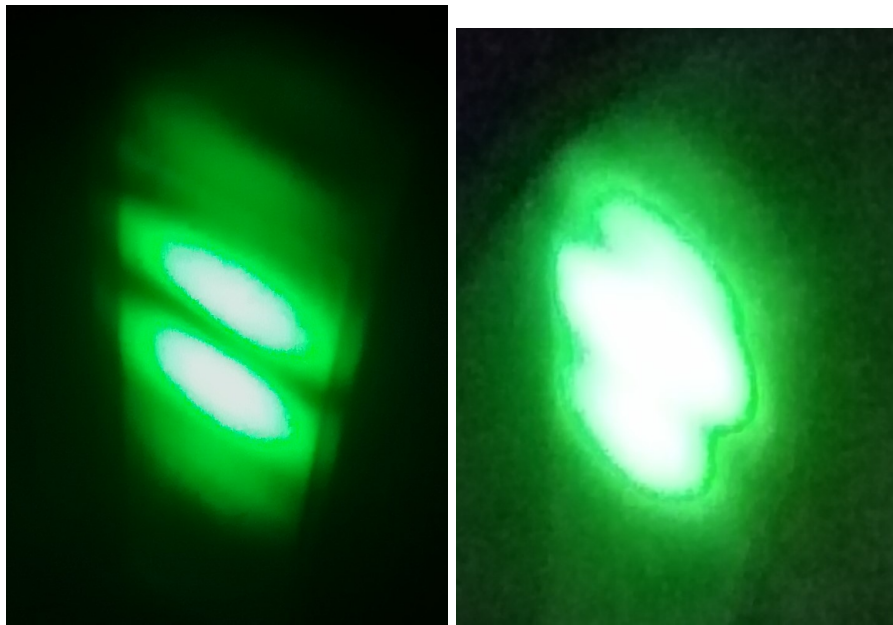
The translating mirror was then further adjusted, with the oscillator running in CW mode, until these interference patterns were as sharp as possible. These sharp patterns are shown in Figure 12c.

When running the oscillator in CW mode, the visibility of the fringes were not very sensitive to movement in the mirror. To increase the precision the oscillator had to be mode locked, so that the tolerance for obtaining fringes was lowered significantly.

In Figure 12d fringes are visible and the oscillator is mode locked. The visibility of these fringes is highly sensitive to moving the translating mirror, and a high precision for zero path length difference is achieved.



(a) The signal exiting the interferometer (b) Weak interference patterns when the when the difference in path length was oscillator was run in CW mode. large.



(c) Sharp interference patterns when the oscillator was run in CW mode. (d) Visible interference pattern when the oscillator was mode locked.

Figure 12: Pictures taken of a screen where the magnified beam was directed after the interferometer. The images display different amounts of interference.

4.2 Raman Measurements

To decide which settings to use with the external oscillator laser, spectra was first obtained using the Raman microscope's internal 785 nm laser. In Figure 13 a spectrum was acquired for 1 second using the 150g grating. The FWHM bandwidth of this peak was determined to be 7.5 cm^{-1} .

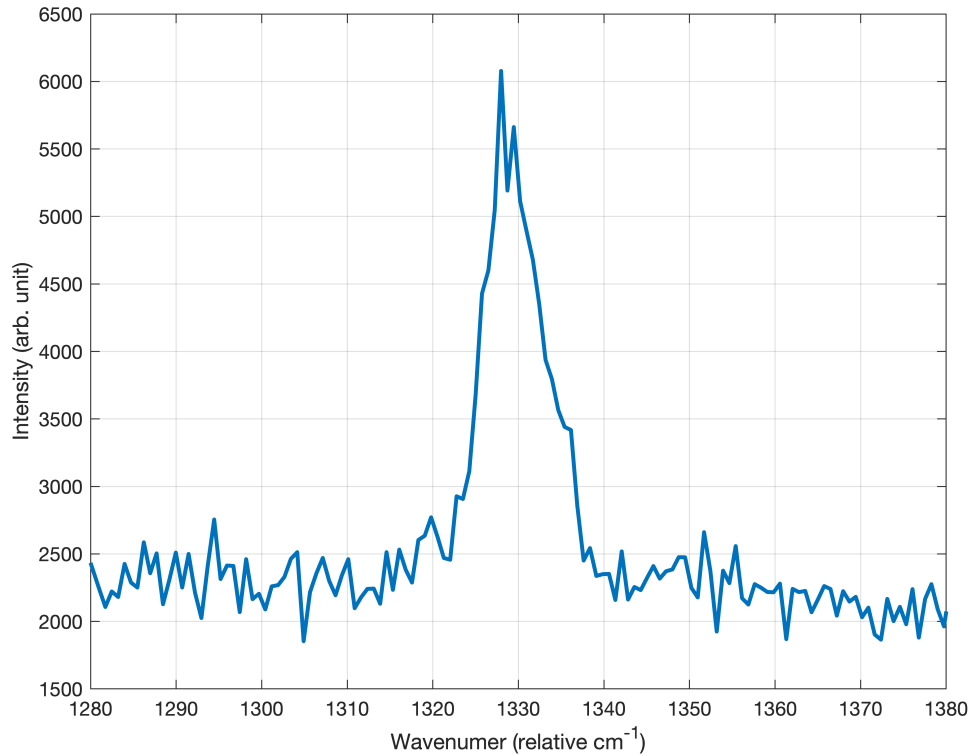
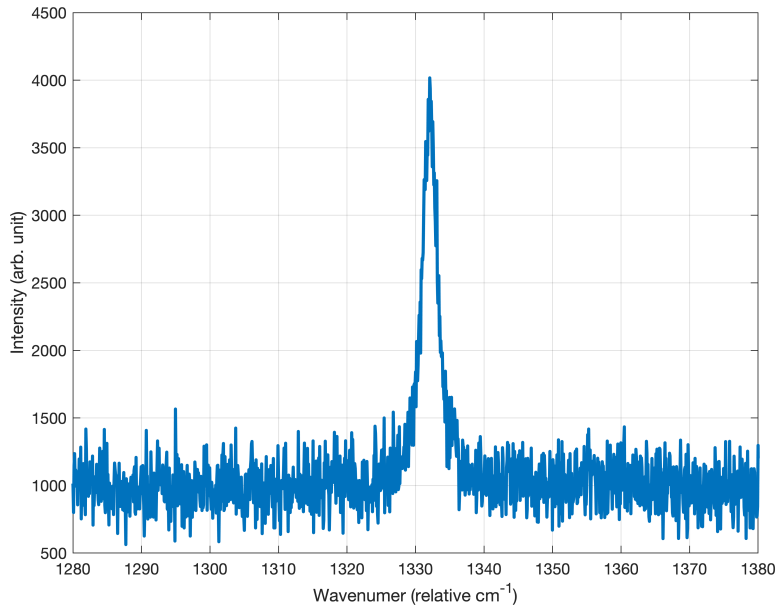
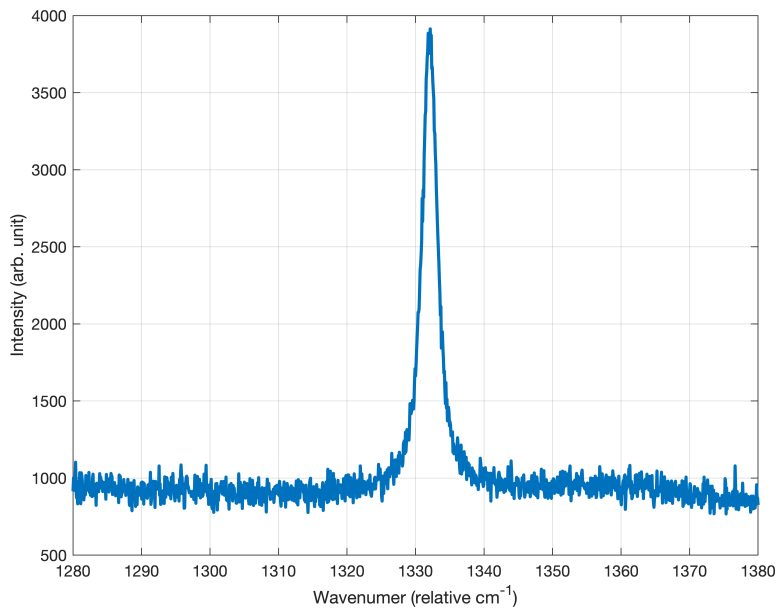


Figure 13: The Raman peak for diamond measured with the internal 785nm laser of the Raman microscope with a grating with 150g/mm.

The same peak was recorded with the 1200g grating with a 10s and a 100s acquisition time, and the result is shown in Figure 14. The FWHM bandwidth of the same peak were in these spectra determined to be 2.5 cm^{-1} . This shows that the 150g grating has a resolution of about 7.5 cm^{-1} , which corresponds to 0.46 nm . From Equation (2.4) with $\lambda = 785 \text{ nm}$, the maximum time delay for resolving an interference pattern with the 150g grating is thus 4.5 ps .



(a) Spectrum acquired for 10s.



(b) Spectrum acquired for 100s.

Figure 14: Spectra of the 1332 cm⁻¹ raman peak in diamond acquired using the Raman microscope's internal 785 nm laser with a 1200g grating.

In Figure 14 it is shown that the signal to noise ratio when acquiring a spectrum for 100 s

is substantially higher than when acquiring for 10 s.

A Raman spectrum of Silicon was then acquired using the external laser as shown in Figure 15.

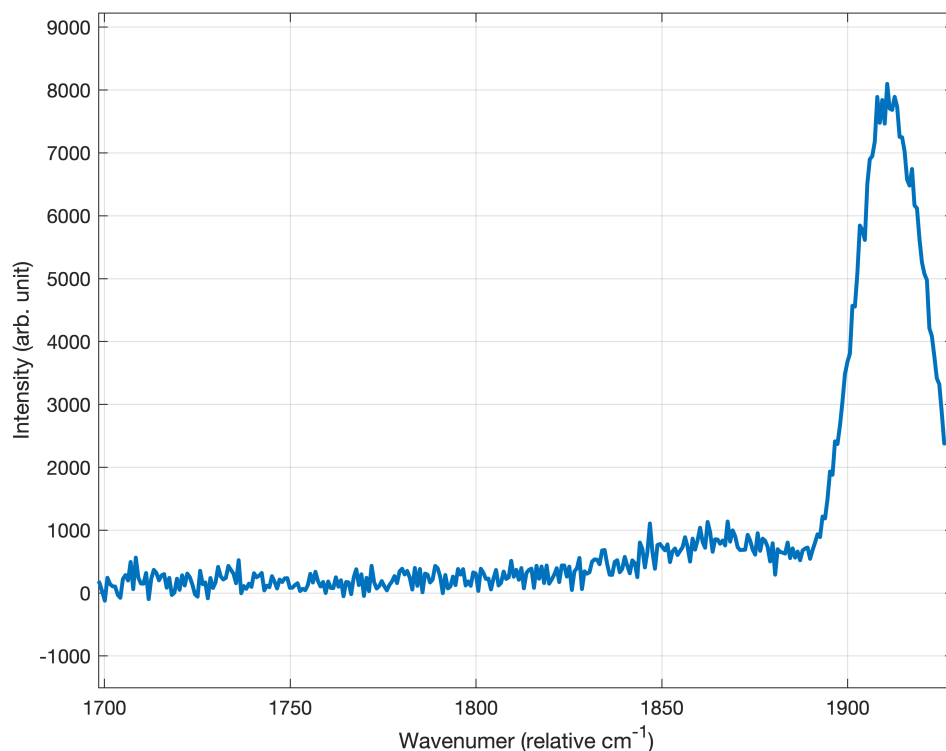


Figure 15: Raman spectrum of Silicon with 150g grating. The peak at 1910 cm^{-1} is a disturbance coming from the Rayleigh peak.

The peak seen at 1910 cm^{-1} doesn't match any Raman peak in Silicon, and is not visible when acquiring spectra with the internal 785 nm laser. It was thereby concluded that this was due to some disturbance. The reason why this peak emerged was not investigated further, but it was probably due to some intensity far from the central wavelength of the oscillator. To mitigate this, a bandpass filter centered around 785 nm with a 3 nm bandwidth was placed before the Raman microscope. An edge filter, which was a longpass filter at around 785 nm, was already included in the Raman microscope. This worked well for filtering out the Rayleigh signal of the internal 785 nm laser since the bandwidth of this laser was very narrow. The pulsed external laser had a much wider bandwidth, and a lot of the Rayleigh signal from this laser leaked through this edge filter. To filter out the Rayleigh signal from the pulsed laser a cut-on filter at 850 nm was placed after the sample.

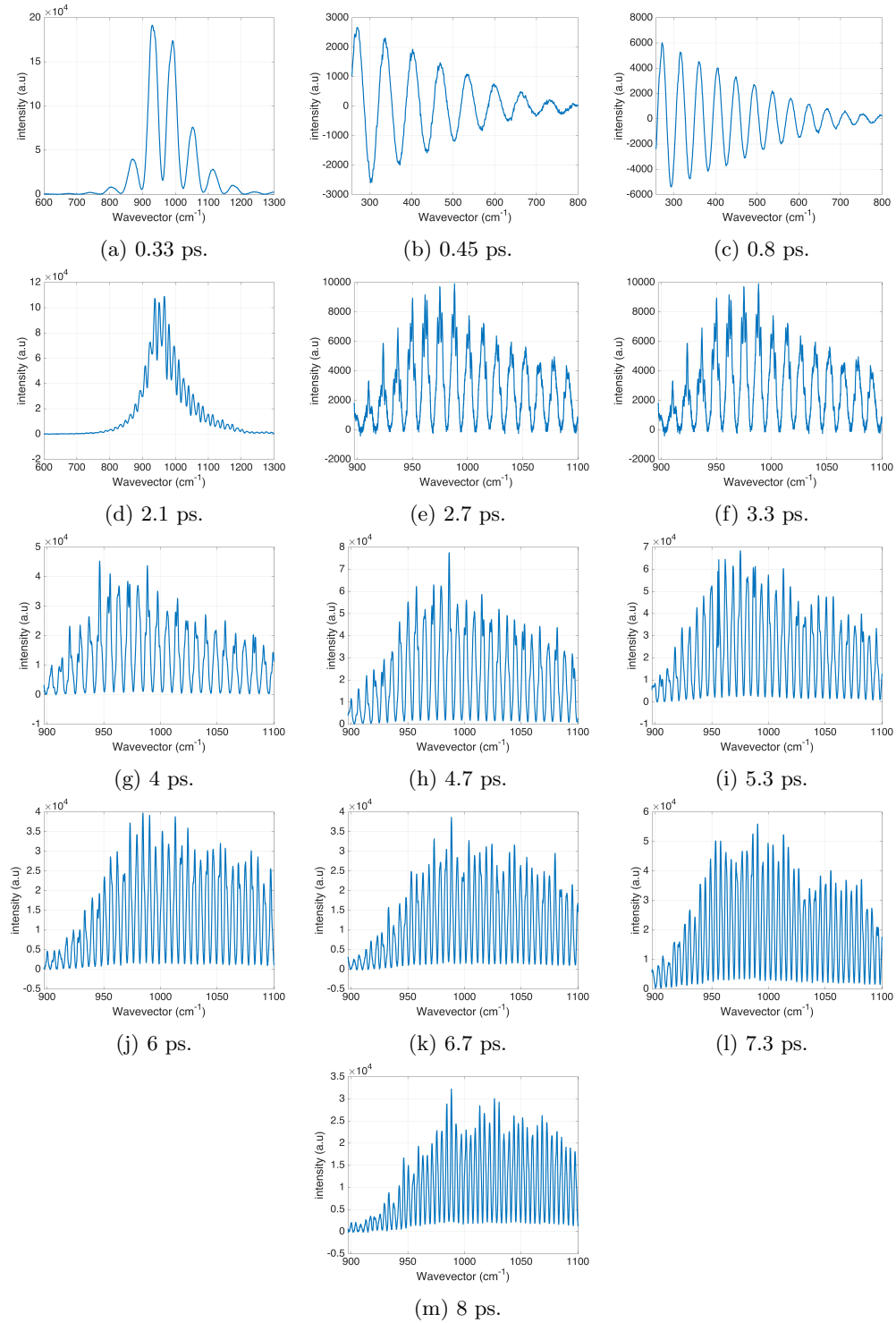


Figure 16: Spectra taken of the Rayleigh peak for different pulse delays. The reason that (b) and (c) look different is that a 850 nm longpass filter is inserted after for the rest of the spectra the sample which only lets the long wavelength tail of the Rayleigh signal through. Spectra e) through m) were taken with the 1200g grating.

The period of the fringes is not material dependent, and is not specific for the Raman signal. The overlap of the pulses was very precisely optimized and spectra were taken of the Rayleigh signal with different pulse delays. This is shown in Figure 16. The periods of these fringes were measured and plotted with the theoretical period shown in Figure 5, the results are shown in Figure 17.

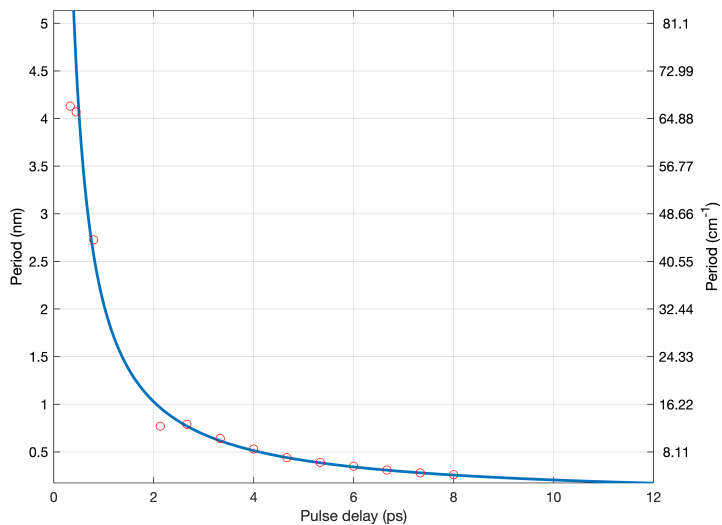


Figure 17: The measured periods of the fringes shown in Figure 16 plotted with red circles together with the theoretical plot shown in Figure 5

In Figure 18 the effect of the cut-on filter can be seen as a ramp, where the half-way point between full transmission and no transmission is at around 930 cm^{-1} . The Raman peak at 1332 cm^{-1} is also visible, and is shown in more detail in Figure 19.

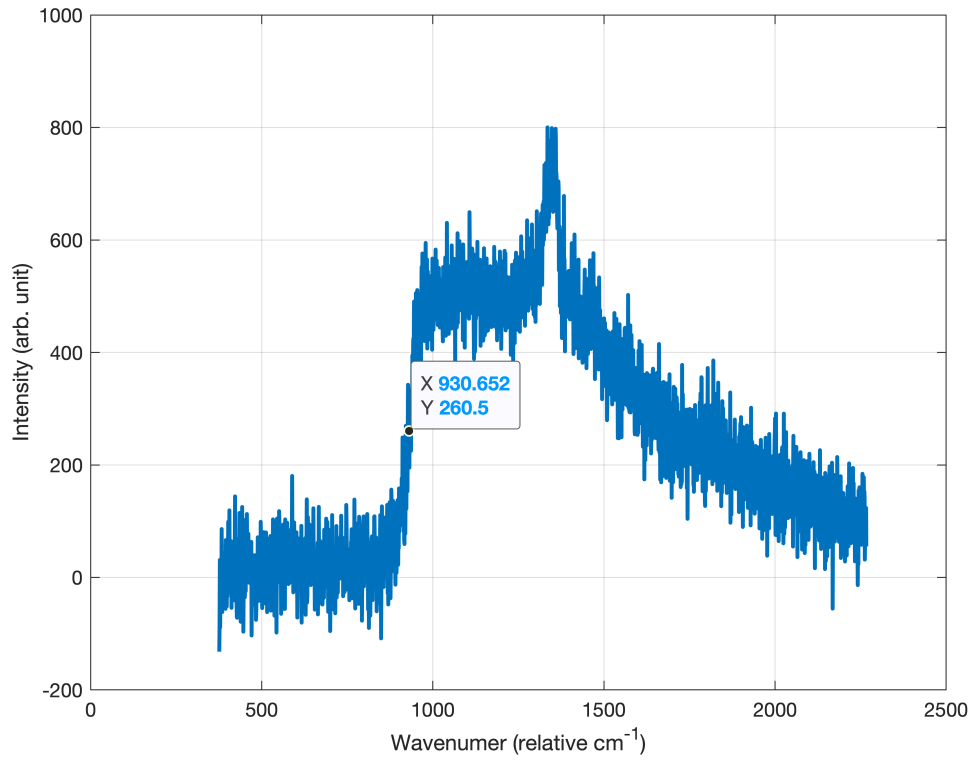


Figure 18: The Raman spectrum of diamond acquired with the external laser using a 150g grating with a 3 nm bandpass filter on the incoming laser light. The data cursor is placed where the transmittance of the cut-on filter is approximately 50%.

The FWHM bandwidth of the Raman peak is measured to be 35 cm^{-1} which corresponds to 2 nm. This is in good agreement with the bandwidth of the interference filter which is 3 nm. This bandwidth is well above the resolution for the grating, which is 0.46 nm, and the peak is well resolved. For these spectra the delay between the pulses in each pulse pair was long enough to not expect any interference pattern since the visibility of the fringes would be too low to detect.

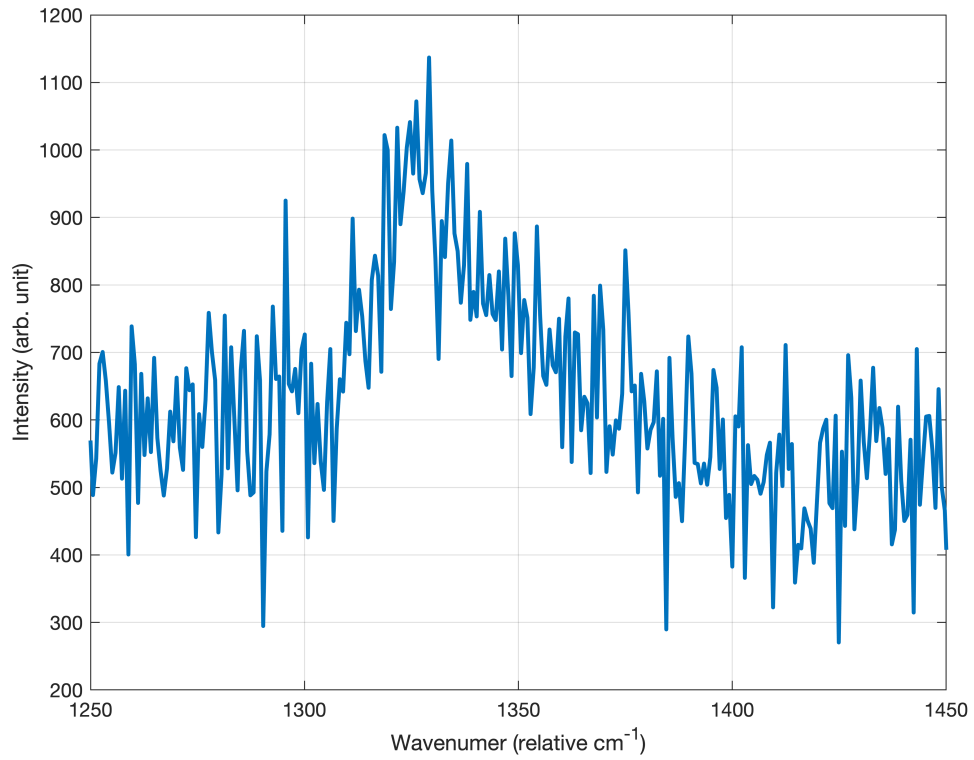


Figure 19: The spectrum of the Raman peak for diamond acquired with the external laser using a 150g grating with a 3 nm bandpass filter.

In Figure 20 a spectrum is shown for the Raman peak in diamond from the external laser using a 10 nm bandpass filter centered around 780 nm. The spectrum is captured using the 150g grating.

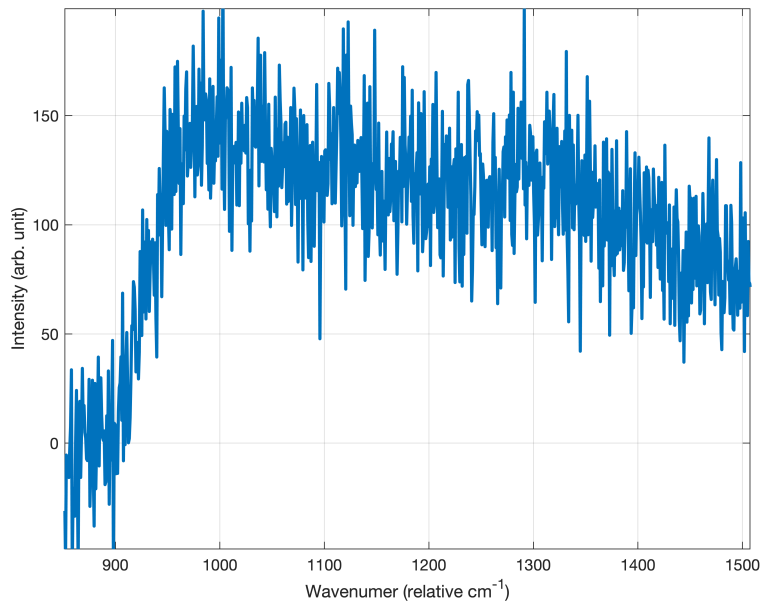


Figure 20: The spectrum of the Raman peak for diamond acquired with the external laser using a 150g grating with a 10 nm bandpass filter centered around 780 nm.

In Figure 21 a spectrum of the Raman peak for diamond is shown which was acquired for 2 hours using the external laser and a 1200g grating. The signal to noise ratio for this spectrum is very low due to the much lower signal strength when using the 1200g grating compared to the 150g.

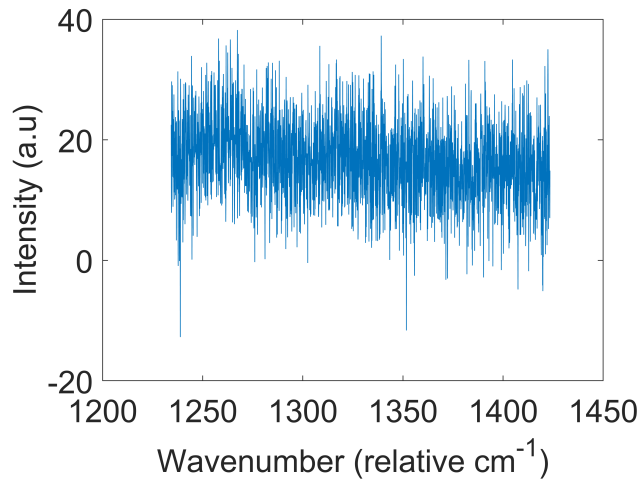


Figure 21: A spectrum of the Raman peak for diamond captured for 2 hours with the external laser on the 1200g grating using a 10 nm bandpass filter centered around 780 nm. The time delay between pulses was 1.5 ps.

In Figure 22 the same spectrum as in Figure 21 is shown, but with a 12 cm^{-1} gaussian filter applied in MATLAB. The purpose of this filter is to reduce the noise and obtain a signal from the data, and when applying the filter some peaks are visible.

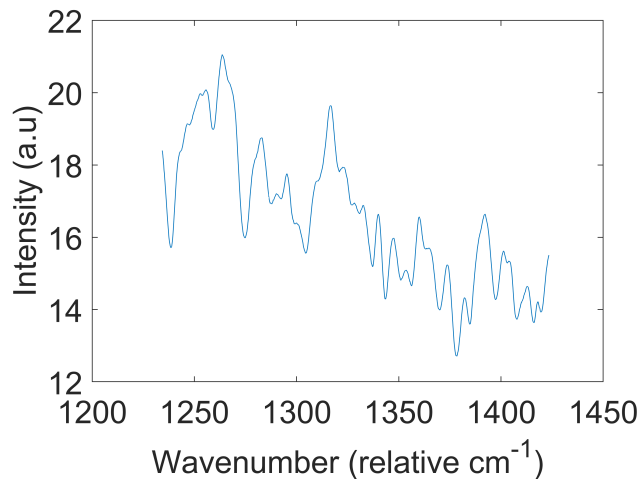
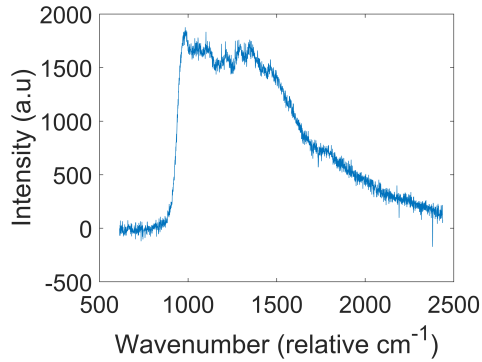
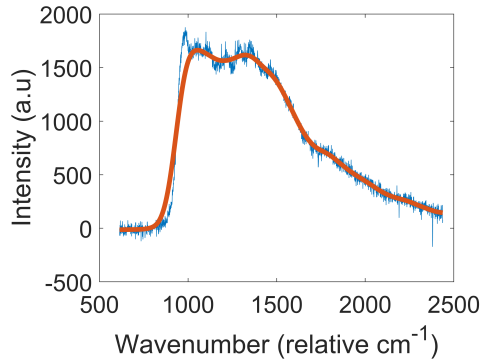


Figure 22: The same spectrum as shown in Figure 21 with a 34 cm^{-1} wide gaussian filter applied.

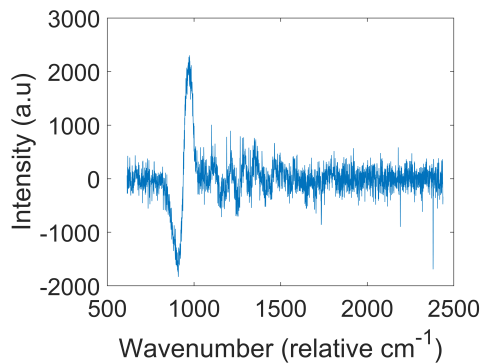
In Figure 23a the spectrum of the Raman peak with 0.33 ps pulse delay acquired with a 150g grating is shown. In Figure 23b this data has been smoothed with a window which is much wider than the predicted oscillations. This smoothed data is then subtracted from the original data to be able to process just the oscillations without being affected by the DC-component which comes from the background fluorescence peak. This is shown in Figure 23c. This data is then cut to remove the peak at 1000 cm^{-1} which comes from the overshoot seen in Figure 23b. This is then multiplied with a Hanning window to get rid of the sharp edges from cutting the data, the Hanning window and the resulting data is shown in Figure 23d.



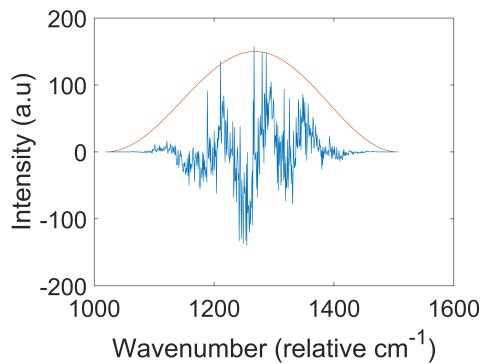
(a) Raw data of the Raman signal with a 0.33 ps pulse delay acquired with a 150g grating.



(b) The raw data is shown in blue and in red the data has been smoothed with a window much larger than the expected oscillations.



(c) The difference of the raw data and the smoothed data.



(d) In red is a Hanning window and in blue is the data after multiplying with this Hanning window.

Figure 23: The spectrum of the Raman peak taken with a 150g grating and a 0.33 ps pulse delay. This data is then processed to be able to Fourier transform the data.

In Figure 24 is the FFT of the data in Figure 23d shown. This has a peak at 0.19 nm^{-1} which corresponds to a period

$$d\lambda = \frac{1}{0.19} = 5 \text{ nm}.$$

The theoretical value of the period is 6.2 nm.

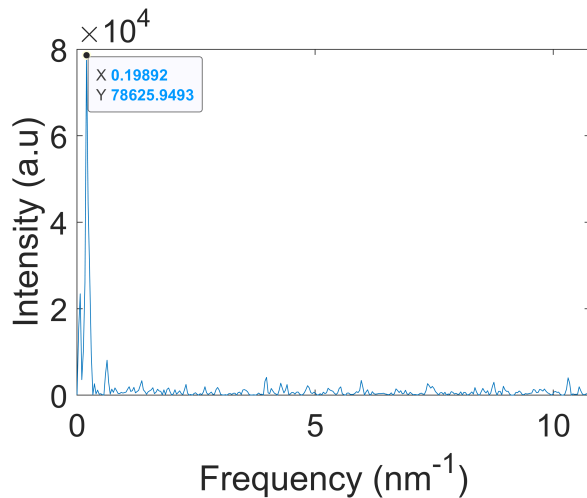


Figure 24: Caption

5 Discussions

The measurements seen in the previous installments using similar setups have been done with around 0.3 ps as the lowest difference in delay between two acquisitions.[18] The interferometer constructed in this thesis could consistently obtain fringe patterns for the mode locked 70 fs laser pulses. This implies that the resolution of the translation stage is well within being able to resolve 0.3 ps differences in pulse delay.

From Figure 17 we can see that the experimentally measured period of the fringes as a function of the pulse delay matches the theoretical expected period very well. The visibility of the fringes in the Rayleigh signal is very high. This means that the overlap of the pulses in the sample is adequate, and also that the delay stage in the interferometer works as intended.

The strength of the background fluorescence seems to be dependant on the total laser power. This means that the fluorescence is as strong for a 30 mW pulse with 3 nm bandwidth as for one with 10 nm bandwidth. Assuming the same pulse shape, the peak of the 3 nm Raman signal will be 3.33 times as high as for the 10 nm wide pulse. The implication of this is that the 10 nm wide pulse will be much harder to distinguish from the background than the 3 nm pulse.

The frequency interference pattern that was sought after with this setup would manifest itself as modulations on a Raman signal without any interference. If at least two full periods should be visible to see a fringe pattern, looking at Figure 5 we see that this can only be achieved for pulse delays below 1.7 ps for a 3 nm bandpass filter. Thus a wider bandwidth filter has to be used to get a wider Raman signal.

As seen in Figure 20 using a wider bandpassfilter of 10 nm greatly reduces the signal to noise ratio of the signal. Compare this with Figure 19 and it is obvious that the signal is clearer for the 3 nm bandpass filter, and it does not seem as though the signal is even discernable from the diamond fluorescence with the 10 nm bandpass filter.

This is a reason to use purer diamond with a lower nitrogen content which could lower the fluorescence signal.

For resolving fringes with a shorter period, the 1200g grating would be useful. As seen in Figure 21 the signal strength for the 1200g grating is much lower than for the 150g grating. Since previous measurements done with similar setups[18] have been done with acquisition times

of 100 s per time delay, it doesn't seem viable to use the 1200g grating as is, since the noisy data acquired had to be acquired for two hours. This might improve if the stability of the interferometer is increased by for example enclosing the interferometer, shielding in from wind currents.

When smoothing the data, as shown in Figure 22, the situation is slightly better, and some characteristics of the signal can be distinguished. A pattern with peaks at 1258, 1290 and 1324 cm^{-1} might be visible, which would correspond to a time delay of 1.3 ps between the pulses, which is close to the actual delay of 1.5 ps for this measurement. Further measurements has to be conducted to verify if this is a repeatable result, or just a random artifact from the measurements. These peaks would also be inside the envelope of a Raman pulse for a laser with a 10 nm wide signal centered around 780 nm. This envelope would span from 1170 cm^{-1} to 1332 cm^{-1} .

In Figure 24 it is shown that it is possible to measure a periodic pattern with FFT which corresponds almost to the theoretical period. This result was also repeated with another spectrum at the same delay. One reason this period does not correspond exactly to the theoretical value is that the uncertainty of the delay stage for short time delays is large as seen in Figure 17.

Since no fringes with high enough visibility to fit a sinusoidal function were observed, the computer programs that were written were never used to actually acquire or process real data. The LabVIEW script was tested without acquiring data and it will be useful for automatically acquiring data in the future. The MATLAB script was tested on simulated data, and worked well for low-noise data sets. For higher noise levels something more sophisticated might be necessary to construct.

6 Conclusions

As shown in Figure 12 the Michelson interferometer is proven to work, and further in Figure 10 it is shown that the overlap is good since the laser spot is circular and there are no signs of there being two spots with bad overlap and in Figure 16 the overlap is good enough to produce a spectral fringe pattern for the Rayleigh signal in the Raman microscope.

Further evidence is shown in Figure 17 where it is demonstrated that the experimental fringe periods correspond well with the theoretical periods and therefore the delay in the delay stage is very precise.

In Figure 19, it is shown that it is possible to achieve a clear Raman signal with the pulsed external laser and in Figure 12 it is shown that the resolution of the spectrometer is good enough to resolve the fringe pattern for sufficiently high time delays.

These building blocks tell us that a working setup for measuring the coherence time of optical phonons is well within reach, and should be achieved in the near future with only a few adjustments.

7 Outlook

Even though the goal of the project, which was to construct a setup to measure the decoherence time of phonons, was not met, many of the necessary steps were completed, and a clear path on how to move forwards has been laid out.

The first major part of the setup, which has been completed and shown to work, is the Michelson interferometer with a computer adjustable translation stage. It has been shown that it is possible to obtain interference patterns from the oscillator laser using this. Both for running the oscillator in CW mode, but also the more challenging achievement of obtaining fringes reliably when running the oscillator mode locked and it has also been shown that interference patterns in the frequency domain can be achieved.

The telescope that was constructed is also sufficient, and the beam diameter has been made small enough to not be cut off by any optical components on its way to the Raman microscope.

The most challenging part, which was to actually obtain a Raman signal using the external laser, has also been solved. This has never been achieved before using this particular Raman microscope.

A checklist on how to go forwards with constructing a functioning setup is presented below.

1. Optimize the oscillator

As is shown in Figure 18 the fluorescence from the diamond sample is stronger for shorter wavelengths. One way to optimize the spectrum from the oscillator is to tune the center wavelength towards longer wavelengths. The Raman peak would be shifted the same amount, and the Raman signal would not have to compete as much with the fluorescence signal. The oscillator's output power can also be optimized. Higher oscillator power would yield stronger Raman signals, and the signal would stand out more from the noise, increasing the signal to noise ratio.

2. Use cut-off filter

To obtain a more powerful signal, and a broader peak, a band pass filter is not wanted. When the band pass filter is removed when the setup is constructed as of the time of writing this report, the Rayleigh signal leaks through the 850 nm cut-on filter and completely overpowers any Raman signal. If a cut-off filter at 800 nm is inserted before the Raman microscope, the wavelengths that leak through the 850 nm cut-on filter would be filtered out, and the band pass filter could be removed. This would both increase the signal to noise ratio, and increase the region where fringes would be visible.

3. Use higher-grade diamond

The strong fluorescence signal observed in the diamond spectrum may be due to high nitrogen content in the diamond.[24] This fluorescence is competing with the Raman signal at the 1332 cm^{-1} peak. Using a purer diamond with less impurities may reduce the signal from fluorescence and thus reduce the background signal.

References

- [1] Xie, G. Ding, D. Zhang, G. Phonon coherence and its effect on thermal conductivity of nanostructures, *Advances in Physics*. **X**(2018).
- [2] Dlott, D.D. Optical phonon dynamics in molecular crystals, *Ann. Rev. Phys. Chem.* **37**(1986).
- [3] Waldermann, F.C. et al. Measuring phonon dephasing with ultrafast pulses using Raman spectral interference, *PHYSICAL REVIEW B* **78**(2008)
- [4] Michelson, A.A. Morley, E.W. On the Relative Motion of the Earth and the Luminiferous Ether , *The American Journal of Science*. **203**(1887).
- [5] S&I. Confocal Raman Microscope - MonoVista CRS+, <http://www.s-and-i.eu/index.php/products/monovista-crs> (Visited 2019-06-06).
- [6] Kim, J.H. et al. Coherent Phonons in Carbon Nanotubes and Graphene, *Chemical Physics*. **413**(2013).
- [7] Saleh, B.E.A. Teich, M.C. Fundamentals of Photonics Chapter 2 - Wave Optics, *Wiley*. (2007).
- [8] Iaconis, C. Walmsley, I.A. Self-Referencing Spectral Interferometry for Measuring Ultrashort Optical Pulses, *IEEE JOURNAL OF QUANTUM ELECTRONICS*. **35**(1999).
- [9] Saleh, B.E.A. Teich, M.C. Fundamentals of Photonics Chapter 9 - Fiber Optics, *Wiley*. (2007).
- [10] Foot, C.J. Atomic Physics, *Oxford university press*. **First edition**(2014).
- [11] Yu, P.Y. Cardona, M. Fundamentals of Semiconductors, *Springer*. **Fourth edition**(2010).
- [12] Saleh, B.E.A. Teich, M.C. Fundamentals of Photonics Chapter 13 - Photons and Atoms, *Wiley*. (2007).
- [13] Saleh, B.E.A. Teich, M.C. Fundamentals of Photonics Chapter 15 - Lasers, *Wiley*. (2007).
- [14] Raman, C.V. A new light, *Indian J. Phys.* **2**(1927).
- [15] Filik, J. Harvey, J. N. Allan, N. L. and May, P. W. Raman spectroscopy of nanocrystalline diamond: An ab initio approach, *PHYSICAL REVIEW B*. **74**(2006).
- [16] Ishioka, K. Hase, M. Kitajima, M. Coherent optical phonons in diamond, *Applied physics letter*. **89**(2006).
- [17] Klemens, P.G. Anharmonic Decay of Optical Phonons, *PHYSICAL REVIEW*. **148**(1966).
- [18] Waldermann, F.C. et al. Measuring Phonon Dephasing with Ultrafast Pulses, *arXiv*. (2008).
- [19] Lee, K.C. et al. Comparing phonon dephasing lifetimes in diamond using Transient Coherent Ultrafast Phonon Spectroscopy, *Diamond & Related Materials*. **19**(2010).
- [20] THORLABS. Retroreflecting Hollow Roof Prism Mirrors , https://www.thorlabs.com/newgrouppage9.cfm?objectgroup_id=10007. (Visited on 2019-06-06).

- [21] Brabec, T. Spielmann, Ch. Curley, P.F. Krausz, F. Kerr lens mode locking, *Optics Letters*. **17**(1992).
- [22] Yeffet, S. Pe'er, A. A Review of Cavity Design for Kerr Lens Mode-Locked Solid-State Lasers, *Appl. Sci.* **3**(2013).
- [23] Smith, P.W. Mode-Locking of Lasers, *Proceedings of the IEEE*. **58**(1970).
- [24] Schirhagl, R. et al. Nitrogen-Vacancy Centers in Diamond: Nanoscale Sensors for Physics and Biology, *Annu. Rev. Phys. Chem.* **65**(2014).

8 Appendix

8.1 Alignment procedure for Michelson interferometer

The flip mount had adjustments both to adjust the angle to the incoming beam, and to adjust the angle the beamsplitter made with the horizontal plane. The angle the beamsplitter made with the horizontal plane affected the angles the outgoing beams made with the horizontal plane, and also the angle with respect to the horizontal plane of the beam that was split to mirror M2 in Figure 7. This angle adjustment was necessary both to ensure that the outgoing beams had the same height and the same angle with respect to the horizontal plane.

To adjust the interferometer an alignment laser was used to make the coarse adjustments. The alignment laser was placed approximately with the same height and angle that the oscillator beam would have when it entered the setup. Two apertures were placed with the same height with a distance of 65 cm. These were placed to ensure that the incoming beam was parallel to the horizontal plane.

The first adjustment was to ensure that mirror M1 was perpendicular to the horizontal plane. To achieve this the beamsplitter was flipped and the laser light was directly aimed at the mirror. The openings of the apertures were closed to a minimum to ensure that the incoming beam was as small as possible. The tilt of the mirror was then adjusted until the outgoing beam passed through the same two apertures as the incoming beam.

The next step was adjusting the beamsplitter. This was done by mounting two apertures after the setup angled 90 degrees from the initial incoming laser beam. These apertures had the same height as the first two apertures. The flip mount was then unflipped which split half the intensity of the outgoing beam from the adjustable arm towards the two apertures after the interferometer. The path of the mirror M2 was blocked to more easily discern the correct laser beam. The two rotation directions of the beamsplitter were adjusted until the beam passed through both apertures.

Finally the mirror M2 was adjusted. This was achieved by still keeping the flip mount unflipped. The path of mirror M1 was blocked and the path of mirror M2 was unblocked. Half the intensity of the outgoing beam from this mirror was allowed to pass through the beamsplitter. The vertical tilt and also the sideways position of this mirror was adjusted until this beam also passed through the two apertures placed after the setup.

8.2 Matlab code

8.2.1 Fitting data to trigonometric function

```
function [fitSignal a, b]= fitSine(lambda,signal,mode)

% Starting wavelength at 0.
    lambdanorm=lambda-min(lambda);

    if strcmp(mode, 'manual')
        figure();
        hold on;
        plot(lambdanorm, signal, '.');
% Making user chose 2 adjacent peaks.
        [x,y]=ginput(2);
```

```

    % Calculating the estimated period.
    period=abs(x(1)-x(2))
end
% trying to automate
if strcmp(mode, 'automatic')
[peaksPos peaksWavelength]=findpeaks(signal,lambda,'
    MinPeakWidth',0.05);
waveLengthVector=peaksWavelength(2:end)-peaksWavelength(1:end
    -1);
period2=(peaksWavelength(end)-peaksWavelength(1))/(length(
    peaksWavelength)-1);
period=median(waveLengthVector);
%period=(period1+period2)/2;
end
% Creating function with 4 constants to fit.
fitFunc=@(b,lambda) (b(1).*sin((2*pi*lambda./b(4))+b
    (2))) +b(3);
% Introducing bounds on constants.
lb=[0, -2*pi, -inf, period/2];
ub=[inf, 2*pi, inf, period*2]; % Phase should obviously be 0
    to 2pi, -pi to pi or -2pi to 0, but -2pi to 2pi works best
    .
% Calculating constants by Least Square Fitting.
[coeffs,RESNORM,RESIDUAL,EXITFLAG,OUTPUT]=lsqcurvefit(fitFunc
    ,[max(signal)-min(signal), -1, mean(signal),period],
    lambda,signal,lb,ub);
if RESNORM>50
    [coeffs,RESNORM,RESIDUAL,EXITFLAG,OUTPUT]=lsqcurvefit(
        fitFunc,[max(signal)-min(signal), -1, mean(signal),
            period2],lambda,signal,lb,ub);
end
% Returning signal and coefficients.
fitSignal=coeffs(1)*sin(2*pi*lambda/(coeffs(4))+coeffs(2)
    )+coeffs(3);
a=coeffs(3);
b=coeffs(1);
end

```

8.2.2 Constructing simulated data, automating fitting, calculating visibilities and plotting the visibility

```

%% initiate constants and standard vectors
close all;
% Number of curves, number of measurement points.
m=8;
n=5000;
% Vector with pulse delays, vector with wavelengths.
delayVect=[2, 3.4, 4.7, 6, 7.4, 8.7, 10, 11.4];

```



```

% Vector with wavelengths starting at 0.
lambda=linspace(903,909,n);
lambdanorm=lambda-min(lambda);
% Initiating matrix with signals.
SignalsMatrix=zeros(m,n);
% Matrix with amplitudes and number of peaks for each signal.
CoeffMatrix=[1.75 3.5;1.6 4.8; 1.5 6; 1.4 7.5; (2.8-1.6) 8.5;
    (2.75-1.7) 9.7; (2.75-1.75) 10.8; (2.55-1.75) 12];
% Size of "measurement error".
ErrorMagnitude=0.05;
%% construct signals matrix 1
% Calculating exponential decay of signal amplitude.
alpha=log(0.75/2)/(-9.4);
for k=1:m
    % Initiating new error value.
    r=normrnd(0,ErrorMagnitude,[1,n]);
% Construction of cos-functions with error.
SignalsMatrix(k,:)=r+2.125*exp(-alpha*(delayVect(k)-2))*cos(rand
    *2*pi+(1/(max(lambda)-min(lambda)))*lambda*CoeffMatrix(k,2)*2*
    pi);

end

%% construct signals matrix 2
% Initial and final visibility from paper.
visi=0.75;
visf=0.2;
% Mean amplitude and cos-amplitude.
A00=2.25;
A10=visi*A00;
% Exponential decay factor.
alpha=log(visf/visi)/(-9.4)
for k=1:m
    % Initiating new random number.
    r=normrnd(0,ErrorMagnitude,[1,n]);
% Constructing cos-functions with error.
SignalsMatrix(k,:)=r+A00+A10*exp(-alpha*(delayVect(k)-2))*cos(
    rand*2*pi+(1/(max(lambda)-min(lambda)))*lambda*CoeffMatrix(k
    ,2)*2*pi);

end

%% Fitting one curve to data (not used as of now)
close all;
figure();
% Choosing which curve to fit.
whichcurve=1;

```

```

plot(lambdanorm, SignalsMatrix(whichcurve,:),'.') ;
    [x,y]=ginput(2);
period=abs(x(1)-x(2));
fitFunction=@(b,lambdanorm) (b(1).*sin((2*pi*lambdanorm./b(4)
    )+b(2))) +b(3);
lb=[0, 0, -inf, 0];
ub=[inf, 2*pi, inf, inf];
coeffs=lsqcurvefit(fitFunction,[max(SignalsMatrix(whichcurve
    ,:))-min(SignalsMatrix(whichcurve,:)),-1,mean(
    SignalsMatrix(whichcurve,:)),period],lambdanorm,
    SignalsMatrix(whichcurve,:),lb,ub);
hold on;
plot(lambdanorm,coeffs(1)*sin(2*pi*lambdanorm/(coeffs(4))+
    coeffs(2))+coeffs(3));

%% Fitting trig function to data and calculating visibility
close all;
% Initiating visibility vector.
visibilityVect=zeros(1,m);

for k=1:m
    % Calling fitSine function to fit a sine to data.
    [signal, a, b]=fitSine(lambda,SignalsMatrix(k,:),'automatic')
    ;
    % plot(lambdanorm,signal);
    % Calculating visibility for sine curve.
    visibilityVect(k)=b/a;
end

%% Re-do fitting
% Redo- fitting if one fit turned out bad.
whichcurve=5;
close all;
[signal, a, b]=fitSine(lambda,SignalsMatrix(whichcurve,:),'
    manual');
hold on;
plot(lambdanorm,signal);
visibilityVect(whichcurve)=b/a;

%% Plot visibility
close all;
% Plotting calculated visibilities for the sine functions.
plot(delayVect, visibilityVect, '.', 'MarkerSize',15)
% Fitting exponential curve to experimental data.
curve=coeffvalues(fit((delayVect-delayVect(1))',visibilityVect','
    exp1'));
a=curve(1);
alphaVisibility=-curve(2);
hold on

```

```

plot(delayVect,a*exp(-alphaVisibility.*(delayVect-delayVect(1))))
% Calculating lifetime from decay constant.
lifetime=1/(alphaVisibility)

%% Plot interference curves

close all;
figure();
for k=1:4
subplot(4,2,2*k-1)
plot(lambda,SignalsMatrix(k,:))
ylabel(delayVect(k))

subplot(4,2,2*k)
plot(lambda,SignalsMatrix(k+4,:))
ylabel(delayVect(k+4))

end

%% Trying to automate finding frequency

close all

plot(lambda,SignalsMatrix(8,:))
[peaksAt positionPeaks]=findpeaks(SignalsMatrix(8,:),lambda,'
    MinPeakWidth',0.1)

```

8.3 LabVIEW code

The front end, which is the interface the user sees when using the LabVIEW program for the translation stage is seen in Figure 25. The back end, which is where the programming is done is seen in Figure 26. Most of the code was already available as a template included for the translation stages. The modifications done to the code were numerous though, including making the translation stage being able to take discrete steps and staying at each step for a set amount of time by using a for loop, including code to make the program use the correct files for the specific translation stage, calculating the number of steps by allowing the user to specify the step size and the end destination, and more.

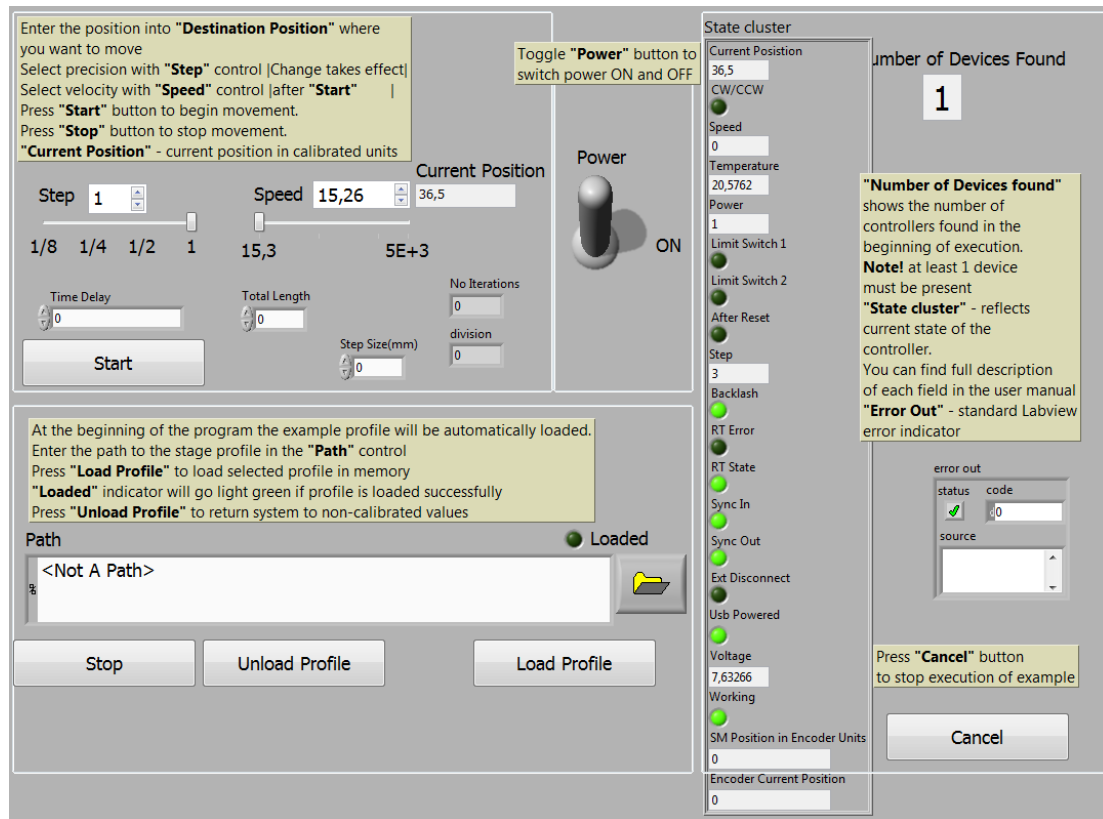


Figure 25: The front panel when using the LabVIEW program to control the translation stage.

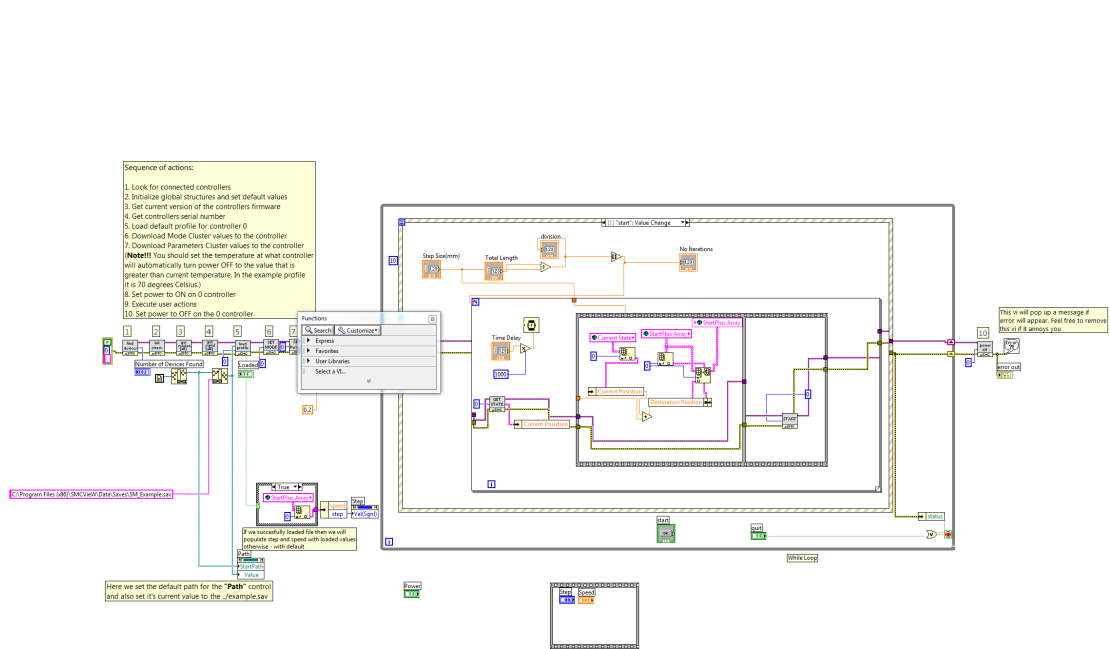


Figure 26: The back end of the LabVIEW program used to control the translation stage.

The full code is not shown in Figure 26, since the block to the right has several layers depending on which trigger has been activated, and many of the layers are uninteresting.